Clockwork Orangutan: microRNAs, thermoregulatory tradeoffs, and the evolution of brain size.

Bastian Fromm*, PhD

The Arctic University Museum of Norway

UiT- The Arctic University of Norway 9037

Tromsø, Norway

Thomas Sorger, PhD

Department of Biology

Roger Williams University

Bristol, Rhode Island 02809, USA

*** corresponding author**

SUMMARY

Hypotheses to account for the energy demand associated with the disproportionate increase in brain size in the human lineage have not considered thermoregulatory constraints. Unlike log-based specific metabolic rates (*sMR*s), the distribution of cellular *MR*s (*cMR*s) can be matched to those of relevant traits, like body temperature and the number of microRNA families (*mirFam*). We demonstrate that the *mirFam*-based *cMR*s of the four most thermogenic organs (kidney, heart, liver and brain) form a core with a joint *cMR* that scales as $M^{0.52}$, as predicted by a comprehensive biophysical model of thermoregulation in homeotherms. Across Euarchontoglires, core organs do not evolve independently: while all organ sizes increase with body size, brain and liver proportions in the core are strictly anti-correlated, as are their *cMR*s, echoing the expensive tissue hypothesis. We propose a positive feedback relationship between larger brain size and greater reliability of the energy supply, on the one hand, and decreasing reliance on liver gluconeogenesis on the other. The corresponding logistic model detects size adaptation to a low-energy regime among the smallest primates and, among the primates with the largest brains, thermoregulatory adaptation to the limit on the rate of heat dissipation.

INTRODUCTION

Brain and liver are the two most energy-demanding tissues in mammals, each accounting for ~20% of resting metabolic rate (*rMR*) in humans (6% and 52%, respectively, in mouse) (Elia 1992; Wang et al 2012; Kummitha et al, 2014). The size of the human brain represents a four-fold increase relative to those of other great apes, which in turn are three-fold larger than the brains of gibbons (Smaers et al, 2021; Grabowski et al, 2023; Shao et al, 2023). Since the sizes of the four most thermogenic organs (kidney, heart, liver and brain) scale more or less strictly according body size (Wang et al, 2012), an increase in the absolute size of the brain cannot be accounted for by a decrease in any of the other three organs ("expensive tissue hypothesis" of Aiello and Wheeler, 1995) (Navarette et al, 2011).

Consequently, for a given primate size and resting *MR* (*rMR*), the only way to account for the greater lifetime energy demand of a larger brain is to postulate gains in the reliability of the acquisition and assimilation of food, storage of energy reserves, gestation, lactation and infant care (Mascia-Lees et al, 1986; Koteja, 2000; Fonseca-Azevedo and Herculano-Houzel, 2012; Isler and van Schaik, 2012; Isler and van Schaik, 2014; Kuzawa et al, 2014; Pontzer et al, 2016; Simmen et al, 2017; Grabowski et al, 2023; for review, see Heldstab et al, 2022). However, any account of the change in energy balance associated with a larger brain would not be complete without an explanation of the associated change in thermoregulation: for a given body size and *rMR*, a larger brain implies more rapid internal heat generation accompanied by faster blood perfusion in order to maintain temperature homeostasis (Nybo et al, 2002; Kiyatkin, 2007; Wang et al, 2014; Seymour et al, 2019). Interestingly, a model of the energy cost of action potential generation predicts a global minimum between 37º - 42ºC (Yu et al, 2012).

A comprehensive biophysical model of thermoregulation in homeothermic mammals envisions a thermogenic core, on the one hand and, on the other, a periphery combining the properties of transport, diffusion, convection and radiation (Porter and Kearney, 2009). This model predicts that for a mammalian *rMR* that scales as $M^{0.75}$, the thermogenic core will scale as $\sim M^{0.50}$ (Porter & Kearney, 2009). We postulated that the combination of four thermogenic organs of mammals functions as a thermoregulatory core ("core model"), estimated organ-specific cellular *MR*s (*cMR*s) consistent with physiological and phylogenetic models, and found that this joint "core" *cMR* scaled as predicted ($M^{0.52}$). We demonstrate that across Euarchontoglires, increases in the relative proportion of the brain *in the core* are offset by decreases in the relative proportion of the liver. Since the liver is the primary organ of gluconeogenesis, this observation is compatible with the energy reliability theory of brain size evolution.

Physiologically-based cMRs do not correspond to log-based sMRs

Assuming a power law model, we distinguish between

specific *MR*s (*sMR*s): $sMR = m \times M^b$,

where *b* is the slope of log *rMR*/log *M*, and

cellular *MR*s (*cMR*s): $cMR = n \times M^c$,

where *c* is the exponent of mass obtained by maximum likelihood fitting of rMR/M^c to the distribution of a physiologically-relevant trait, such as the number of microRNA families (*mirFam*). Previously we demonstrated that, unlike *sMR*s, *cMR*s are sensitive to body temperature and robust to sample differences in the range of mass (Fromm and Sorger, 2023).

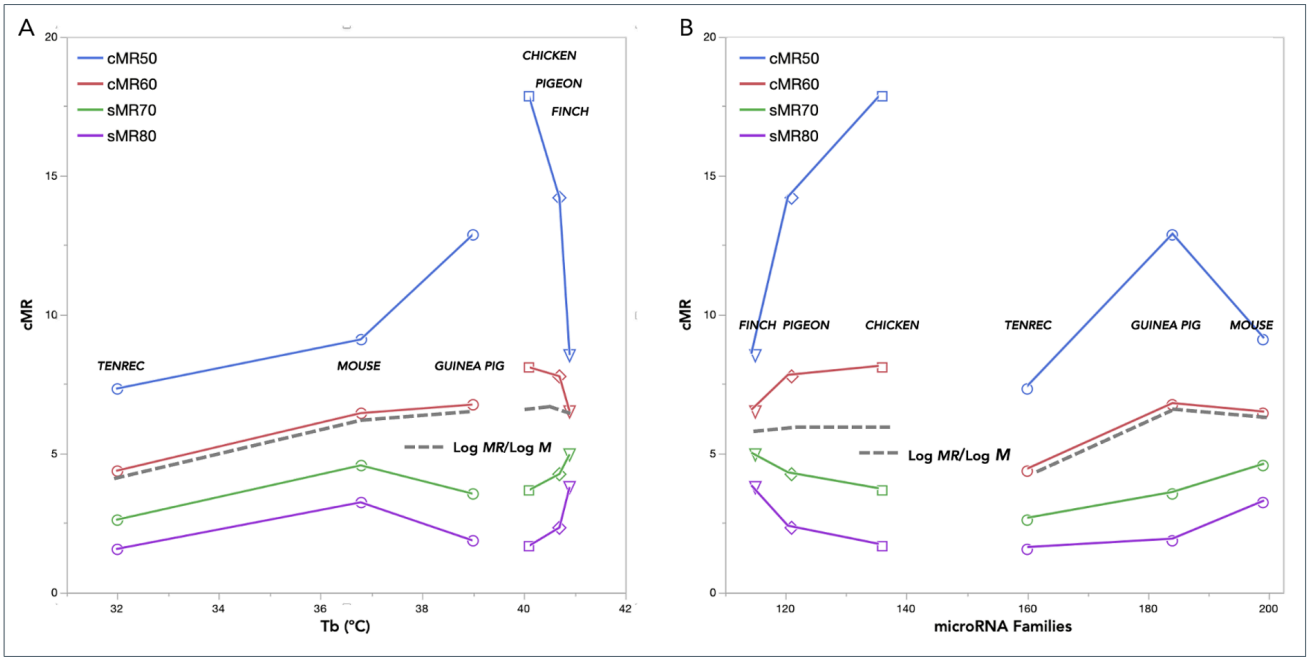

Figure 1. Log-based *sMR*s do not correspond to *mirFam*-based *cMR*s.
Fitting of *cMR*s or *sMR* with respect to (A) body temperature (T_b) or (B) *mirFam*.
Data were drawn from Fromm and Sorger (2023). Hatched lines represent the log-based slopes of the birds (*sMR.64*) and the mammals (*sMR.60*). For the purpose of illustration, a difference in T_b of 0.2º C was applied between pigeon and finch. Note the inversion of *cMR* slopes.

Rates of cellular metabolism depend on traits that do not scale logarithmically, such as body temperature (T_b) or the rate of protein synthesis, for which the species-specific number of microRNA families (*mirFam*) may serve as proxy (Fromm and Sorger, 2023). Furthermore, *cMR*s will vary by tissue type and differ between tissues that are renewable or post-mitotic. The rank order of *cMR*s can be matched to non-logarithmic traits by variable allometric scaling, while the rank order of log-based *sMR*s is fixed according to species size (Figure 1). Thus cellular *MR*s determine not only the overall slopes of these relationships, but also the rank order of *cMR*/trait ratios (Supplementary Figure S1), with implications for models of genetic and phenotypic covariance (Lande, 1979; Felsenstein, 1985; Hansen, 1997; Pagel, 1999; Svensson et al, 2021; Walter and McGuigan, 2023).

In order to develop a thermogenic core model of thermoregulation, we based our estimates of *cMRkdn*, *cMRhrt*, *cMRlvr* and *cMRbrn* in primates on three criteria:

a) size-independent correlation with *mirFam* (physiological relevance);
b) correspondence of the combined *cMR* of these organs with that of the thermogenic core predicted in the biophysical model of Porter & Kearney (2009) (thermodynamic relevance);
c) utility for the unsupervised classification of major primate clades (phylogenetic relevance).

We then examined how tradeoffs in the core between brain and liver were related to the evolution of thermal conductance, divergence of orders and species of Euarchontoglires, and the corresponding changes in body size and organ *cMR*s. Finally, we demonstrate how a logistic model of the relationship between brain size and energy reliability supports the inference of size adaptation to a low energy regime by reduction in size, on the one hand, and thermoregulatory adaptation to the physiological limit on the rate of heat dissipation (hence rate of thermogenesis) in large-brained primates, on the other.

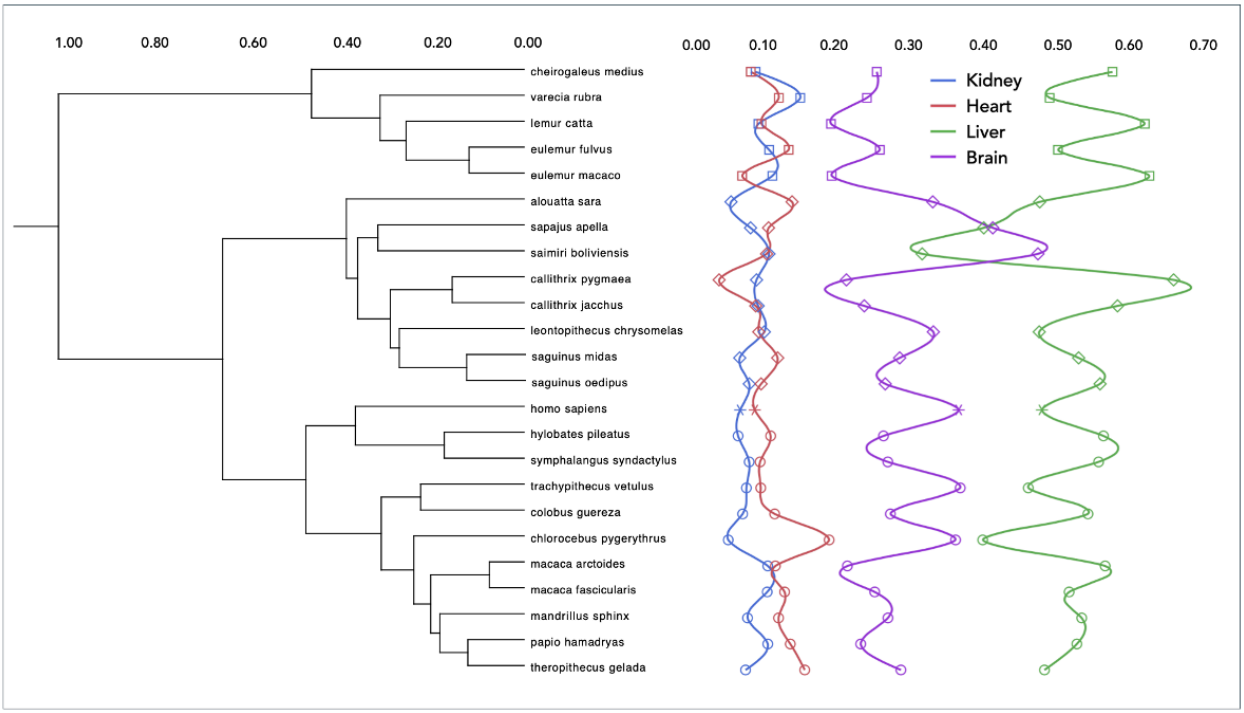

Figure 2. The proportion of brain mass in the core varies reciprocally with that of the liver.

RESULTS AND DISCUSSION

The proportion of brain mass in the core varies reciprocally with that of liver

Of six possible tradeoffs In a core consisting of four thermogenic organs, one major trade off occurs consistently among primate clades, that between brain and liver (Figure 2). A dampened tradeoff between heart and kidney occurs approximately “in phase” with the major tradeoff. Brain and liver proportions in the core also vary reciprocally across 30 additional Euarchontoglires, together with a diminished reciprocity between heart and kidney (Supplementary Figure S2). The observations in primates are summarized geometrically in Figure 3. It is noteworthy that while relative core size (~ $M^{0.50}$) is predicted to decrease with body size (~ $M^{0.75}$) (Porter & Kearney, 2009), the relative core size in humans is greater than that in baboons, which have less than half their body mass.

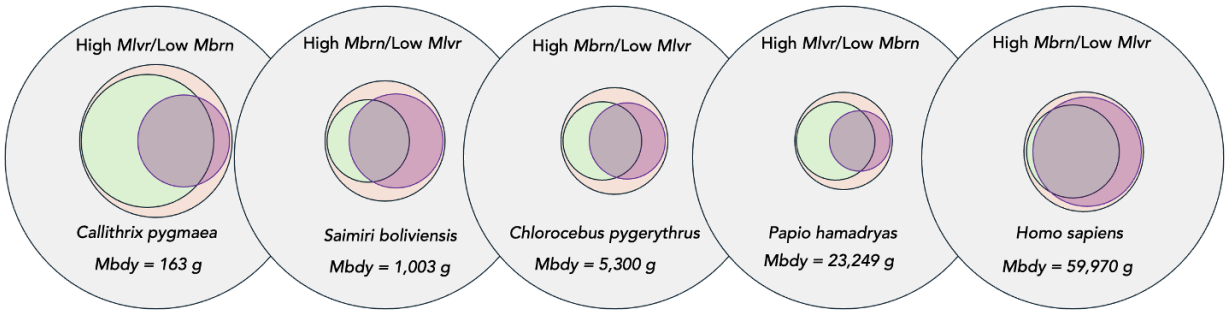

Figure 3. Variation across primates in core size and composition.
The radius of each circle represents a spherical volume corresponding to organ or core mass, scaled to body size (equal circle diameters). The relative proportions of liver and brain are represented by green and purple circles, respectively.

Estimation and physiological relevance of thermogenic organ cMRs

We have previously presented evidence that the number of microRNA families is a statistically and mechanistically credible proxy for the global rate of protein synthesis, which drives 20% of cellular ATP turnover in mammalian cells (Buttgereit and Brand, 1995). We further showed that *mirFam* is an attractor for whole animal *cMR* across the major mammalian clades (Monotreme, Atlantogenata, Laurasiatheria and Euarchontoglires) in a model of stabilizing selection (Fromm and Sorger, 2023). Absent other selective forces, we expected that the diversification of Euarchontoglires would be associated with a steady increase in *cMR* variance with respect to the distribution of *mirFam,* owing to genetic drift and the relaxation of selection.

Figure 4 compares the dependence of *cMR* for each organ on organ size and *mirFam*, together with the log-based *sMR* for each organ. Note the similar trends and inversions among kidney (*kdn*), heart (*hrt*) and brain (*brn*), on the one hand, and liver (*lvr*) and body (*bdy*), on the other.

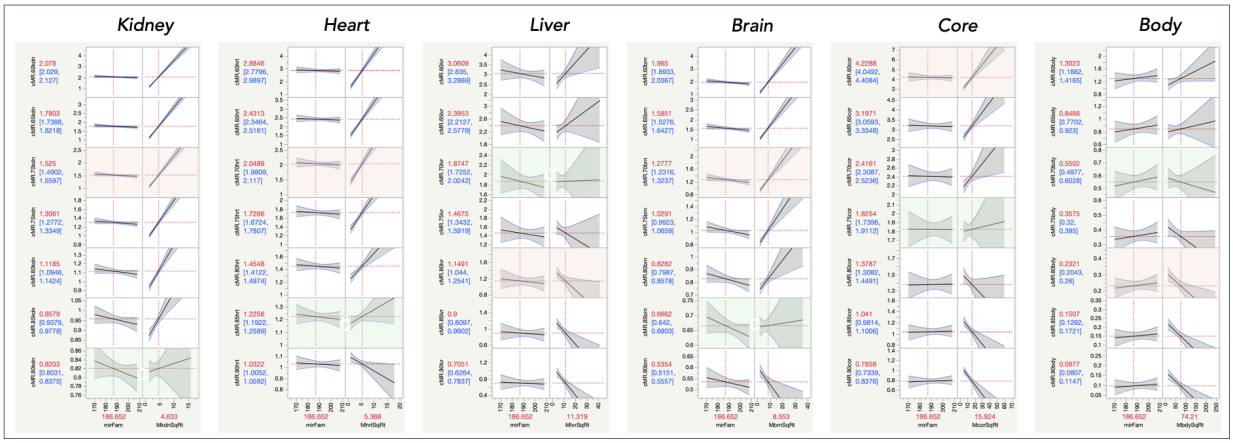

Figure 4. Dependence of *cMR* on √*Morg* and *mirFam* in 23 primates.
√*M*, a natural scale for *cMR*s, yields *P* values several orders of magnitude lower than a log scale. Log-based *sMR* slopes are shaded green, *cMR* slopes are shaded pink.

Figure 5 summarizes these results and compares them to regressions on 27 species of Glires. The Y-axis is an ascending scale of *P* values, which can be interpreted as the degree of release of the constraint of the association with *mirFam*; considering the interval $M^{0.70}$ - $M^{0.80}$, this implies the following order of evolutionary conservation: ***Kdn*, *Hrt* > *Brn* > *Lvr*, *Bdy***. This series comports well with the relative "amplitudes" in the periodic pattern of variation in relative core proportion (Figure 2).

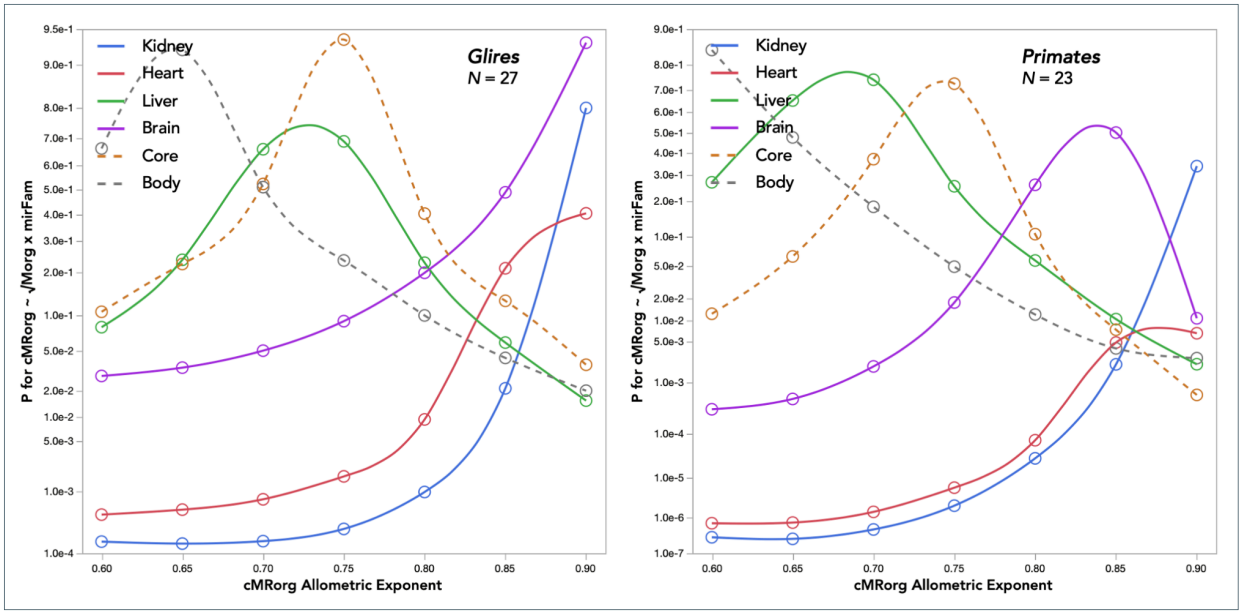

Figure 5. Dependence of *cMR*org on √*Morg* and *mirFam* yields a coherent pattern of variation. Curves were fit by the spline method (*lambda* = 0.00). Note the difference in *P* scales. The primate dataset omitted the largest animal and a small heterotherm (*Homo sapiens* and *Cheirogaleus medius*).

Furthermore, comparing the plots for Glires and Primates, the shift to a lower range of *P* values among primates is consistent with a shorter time frame for the operation of genetic drift. The leftward shift in

the dynamic ranges for liver, and brain cMRs, *i.e.* towards lower allometric exponents, indicates a greater dependence on surface area (Figure 5). Given the higher size range among primates, this shift may indicate a thermoregulatory adaptation corresponding to a faster rate of heat dissipation, an interpretation supported by the observation that vertebrate morphological types, a function of aspect ratios, were significantly related to the number of microRNA families, but not to genome size or the diversity of protein domains (Deline et al, 2018).

Most striking is the inversion of the relationship with *mirFam* of liver *cMR*s (lower *P* values associated with higher *cMR*s), compared to those of kidney, heart and liver (Figure 5). The *cMRbdy* correlation tracks that of the liver, implying that liver is the organ most affected by thermoregulatory adaptation to changes in animal size. Assuming an operating range of *cMR.70* - *cMR.80* for core and whole body, we estimated the relevant organ *cMR*s as *cMR.70kdn*, *cMR.70hrt*, *cMR.70brn* and *cMR.80lvr*, corresponding to the lowest *P* values in this range. Plotting these as a function of primate body size suggests that the anticorrelation between liver *cMR.80* and the other core organs is essential to establishing the overall negative slope of *cMR.75bdy* with respect to animal size (Figure 6). We obtained essentially the same pattern plotting organ *cMR*s against thermal conductance ($\log_2 C_{min}$) in a subset of 16 Euarchontoglires (Supplementary Figure S3), consistent with a thermoregulatory basis.

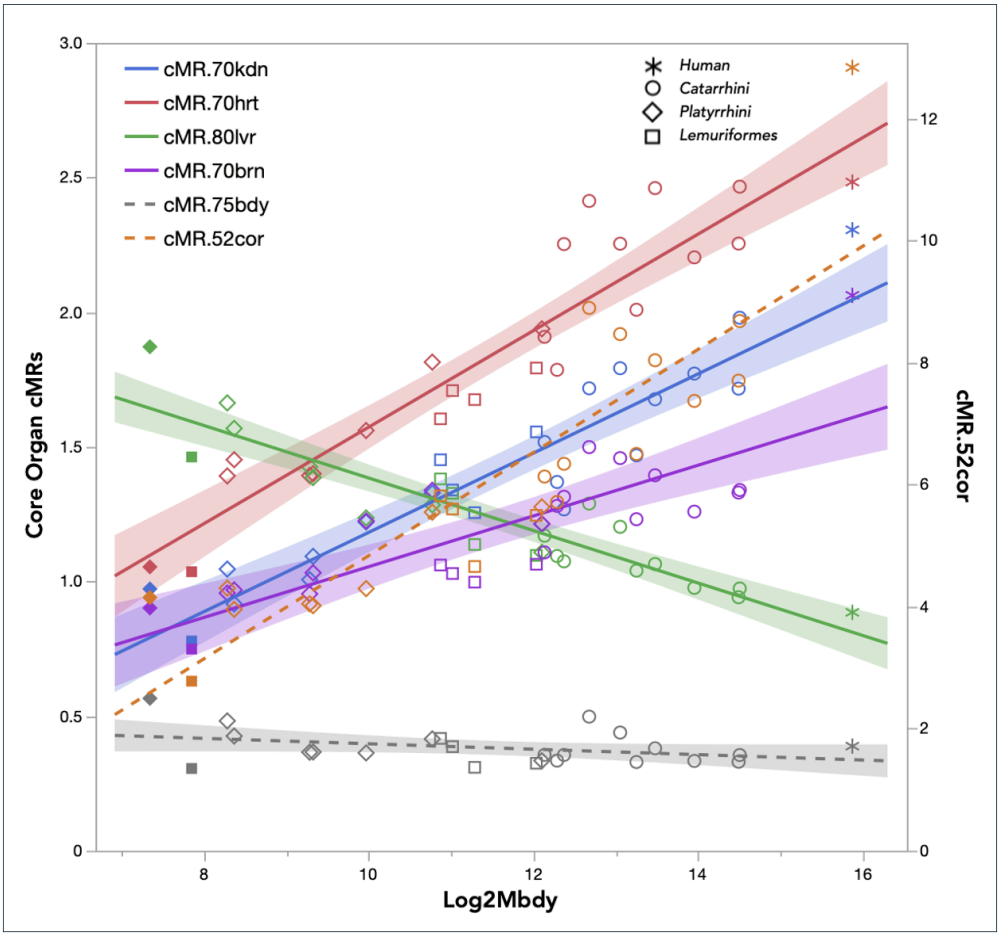

Figure 6. Core organ *cMR*s as a function of body size in 24 primates. Filled symbols represent heterotherms. Shaded bands: confidence interval for each regression line.

We then tested the validity of this combination of core *cMR*s against thermodynamic and phylogenetic models. The biophysical model for thermoregulation of Porter & Kearney (2009) envisions a heat-generating "core" and an ellipsoid surround combining the properties of transport, convection, conduction and resistance. For a steady state, whole animal resting *MR* that scales as $M^{0.75}$, the corresponding rate of core thermogenesis is predicted to scale as ~ $M^{0.50}$ (Porter & Kearney, 2009). As a test of thermodynamic relevance, we compared the predicted allometric scaling of theoretical '*cMRcor*'s consisting of the combination of four thermogenic organs, using either log-based *sMR*s or the estimated *mirFam*-based *cMR*s:

$$\textbf{sMR.Xcor} = (rMRkdn + rMRhrt + rMRlvr + rMRbrn) / (Mkdn + Mhrt + Mlvr + Mbrn)^{X}$$

$$= (a \times sMR.90\text{kdn}) + (b \times sMR.86\text{hrt}) + (c \times sMR.69\text{lvr}) + (d \times sMR.84\text{brn})$$

or

$$\textbf{cMR.Xcor} = (a \times cMR.70kdn) + (b \times cMR.70hrt) + (c \times cMR.80lvr) + (d \times cMR.70brn)$$

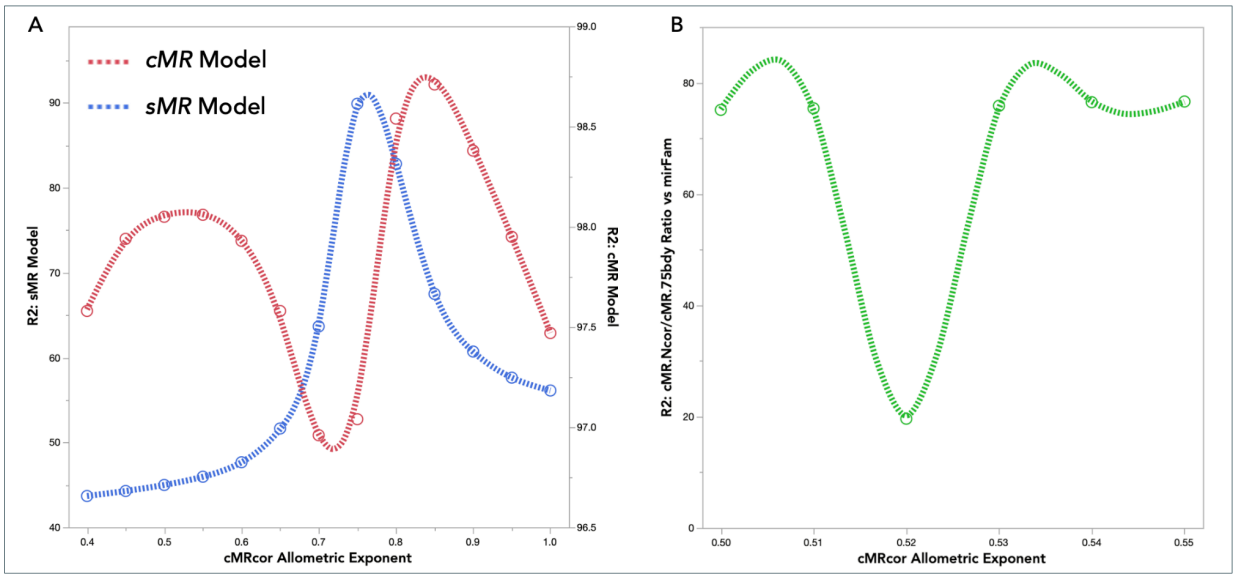

Figure 7. The thermodynamic model of *cMRcor* corresponds to release from *mirFam* constraint.
A. % variation (R^2) of linear models of *cMR*cor predicted by combinations of log-based *sMR*s or *mirFam*-based *cMR*s of the four thermogenic organs for 22 primates (SIMPLS method of partial least squares: deJong, 1993). Note the different scales for the *sMR* and *cMR* models.
B.% variation (R^2) of dependence of the *cMR.Ncor* / *cMR.75bdy* ratio on *mirFam* (51 Euarchontoglires).

The *sMR* model predicted a most probable allometric scaling for this 4-organ core of $M^{0.77}$ (Figure 7), which corresponds to the crossover point for the inversion of slope with respect to mass between *cMR.70* and *cMR.80* (Figures 1 and 4). In contrast, the *cMR* model predicted two possible allometries, one on either side of this inversion, including one that closely matched the predicted allometric scaling (~ $M^{0.50}$) of a thermogenic core in the ellipsoid model of thermoregulation in homeotherms (Porter and Kearney, 2009):

$$
\begin{aligned}
\textit{cMR.52}\text{cor} \quad &= 0.53 \times \textit{cMR.70kdn} \\
&+ 0.38 \times \textit{cMR.70hrt} \\
&+ 0.36 \times \textit{cMR.80lvr} \\
&+ 0.09 \times \textit{cMR.70brn}
\end{aligned}
$$

If *cMR.52cor* represents the optimal rate of thermogenesis and $M^{0.75}$ represents a zone of minimal constraint from association with *mirFam* (Figure 5), this should be reflected when comparing correlations with *mirFam* of *cMR.Xcor / cMR.75bdy* over a range of X. As shown in Figure 7B, the R^2 value for this correlaton exhibited a sharp minimum at $X = 0.52$, supporting our interpretation that optimal thermodynamic model corresponds to minimal constraint by association with *mirFam*.

As a further test of the proposed composition of *cMRcor*, we varied the combinations of organ *cMR*s and found that the estimated *mirFam*-based *cMR*s formed *cMRcor* with the lowest exponent, *i.e.* closest to that predicted by the biophysical model of Porter and Kearney (2009) (Figure 8).

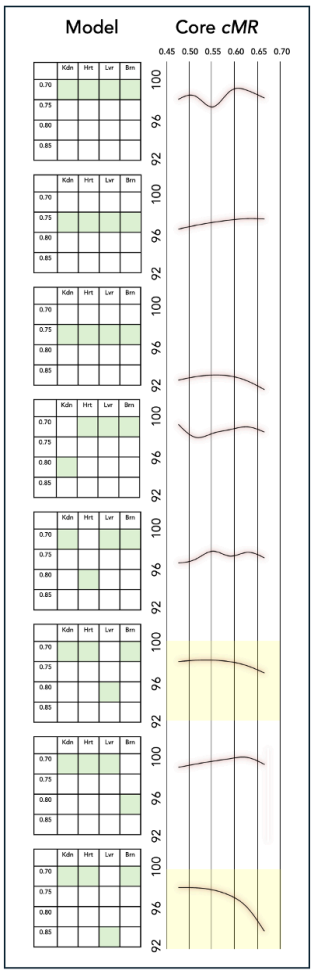

Figure 8. Comparison of core organ *cMR* combinations with respect to the allometric scaling of the corresponding core *cMR*. Each matrix represents one combination of organ *cMR*s, and each trace represents the % variation (R^2) for the predicted *cMRcor* (as in Figure 7).

Two combinations (yellow shading) yielded the lowest optimal core allometric exponent, $M^{0.52}$:

[*cMR.70kdn*, *cMR.70hrt*
***cMR.80lvr*, *cMR.70brn*]**

and

[*cMR.70kdn*, *cMR.70hrt*
***cMR.85lvr*, *cMR.70brn*]**

As a test of phylogenetic relevance, we predicted that the set of core organ *cMR*s that we have estimated would be useful in the unsupervised classification of major primate clades. Expectation

maximization of Gaussian (normal) mixture models allows the inference of a latent grouping variable, in this case phylogenetic clade (Dempster et al, 1977; Celeux and Govaert, 1995). We applied this clustering method to the same 22 primates as in the previous analyses, After varying the *cMR*s for liver, the model with the lowest information criterion was again:

[c*MR.70kdn*, *cMR.70hrt*, *cMR.80lvr*, *cMR.70brn*] (Figure 9).

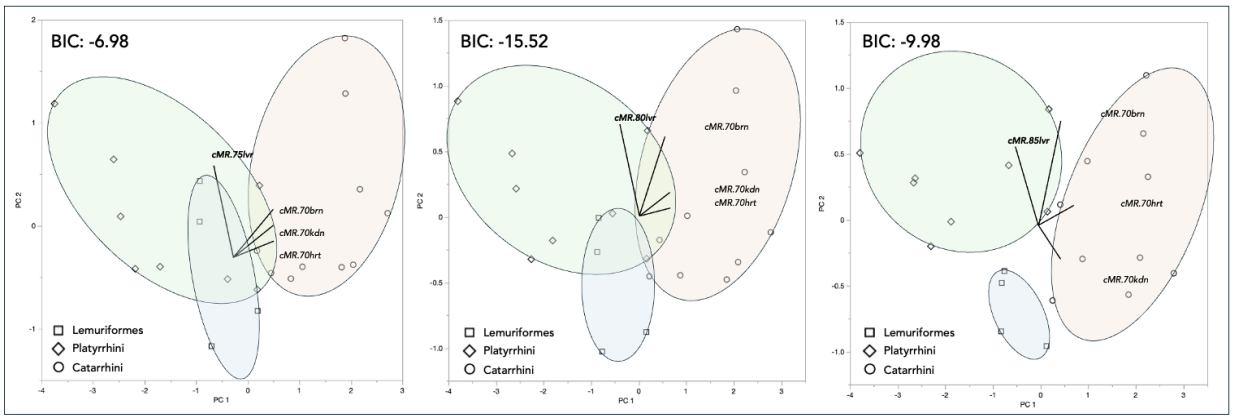

Figure 9. Unsupervised classification of primate clades based on core *cMR* composition. Principal components were calculated from each *cMR* correlation matrix, and membership in two clusters estimated by expectation maximization of their joint probability distributions. Kidney, heart and brain *cMR* = *cMR.70*; liver *cMR*s were varied between *cMR.75lvr* - *cMR.85lvr* (bold type). Ellipses were hand-drawn to include all members of the three phylogenetic clades (N = 22).

While *cMR*s were needed to develop and test the core *cMR* concept, tradeoffs between liver and brain *sMR*s are also readily demonstrable with log-transformed data, *provided that they are ranked according to core size, not body size*. Figure 10 compares the variation in organ size as a function of body mass (Figure 10A) or core mass (Figure 10C). Examination of the residuals of the corresponding regressions reveals a periodic pattern of variation for each organ, corresponding to their relative proportion of body mass (Figure 10B) or core mass (Figure 10D). The periodicity is a function of autocorrelation, as can be easily demonstrated when the analysis is limited to a single pair of organs (Supplementary Figure S4). A consistent tradeoff between brain and liver extending across the entire range is apparent only when organ masses are standardized against core mass (Figure 10D versus Figure 10B). In other words, standardization of log *Mbrn* against log *Mbdy* precludes detection of this tradeoff (Navarette al, 2011).

As a further test of thermoregulatory basis of the observed tradeoffs, we asked how the mass and *cMR* of the core organs were related to thermal conductance in a subset of 16 Euarchontoglires for which C_{min} data were available, including one Lemuriform, one Platyrrhine and one Catarrhine (Khaliq et al, 2014). The evolution of thermal conductance has generally been investigated in the context of adaptation to ambient temperatures, which can be achieved by a combination of adjustments to thermal conductance and resting *MR* (Scholander et al, 1950; Naya et al, 2013; Khaliq et al, 2014; Fristoe et al, 2015; Bennett et al, 2021).

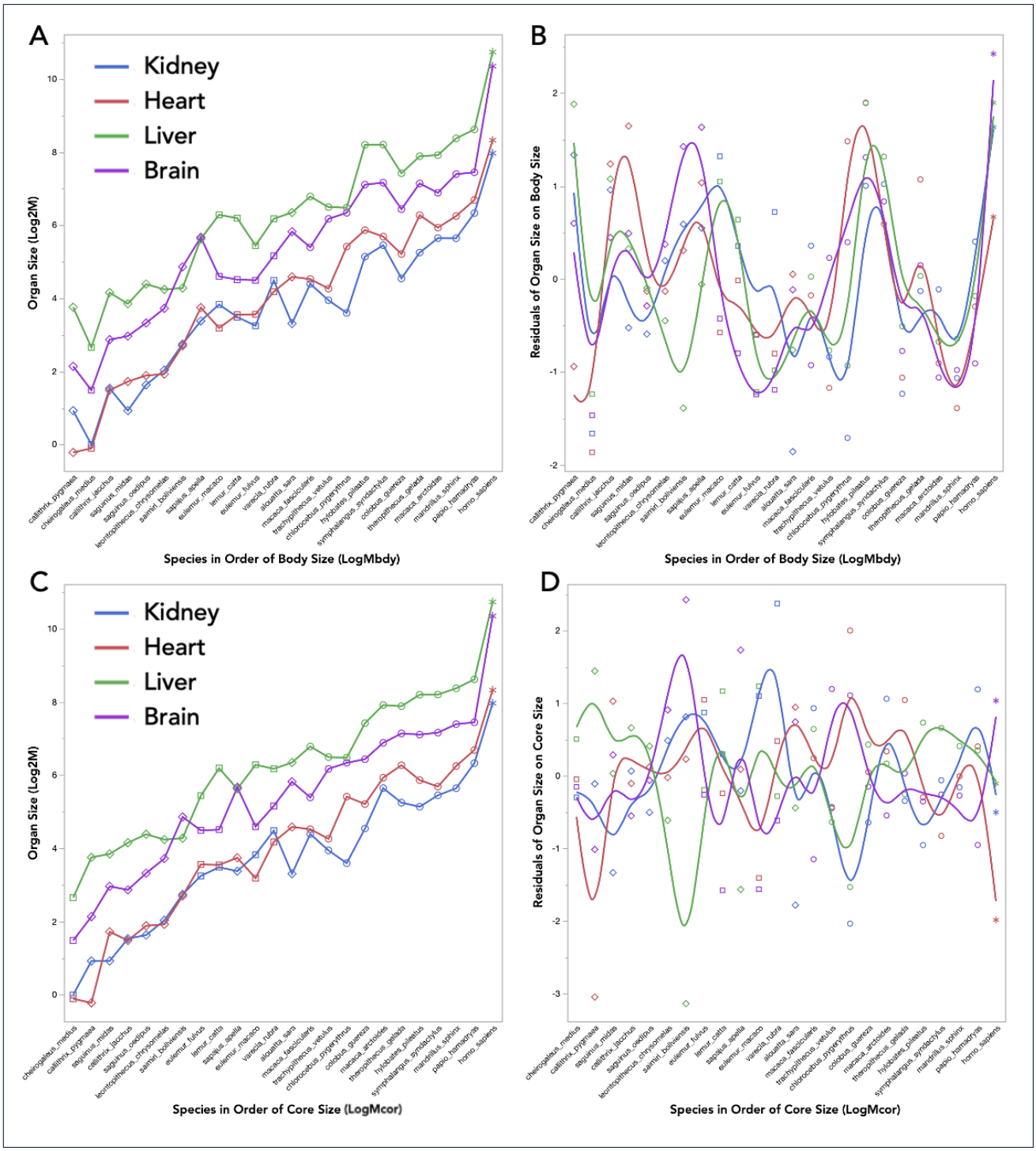

Figure 10. The reciprocal variation between liver and brain is a function of core size.
A and C: Variation of organ size relative to body size and core size in primates.
B and D: Residual variation relative to body size and core size in primates.

While thermogenesis is a core organ property, thermal conductance depends on the whole animal surface and, like organ size, is expected to increase geometrically with body size, as well as with ambient temperature: $\sqrt{Mbdy}$, $\sqrt{Mcor}$ and $\sqrt{Mbrn}$ predicted 67 - 70% of the variation in $\sqrt{C_{min}}$ (6.96e-05 > P > 3.40e-05; N = 16), or 52 - 58% of the variation when using log-transformed values.

In this case, tradeoffs in the core organ *cMR*s might be detected as a function of C_{min}, but not not tradeoffs in organ mass. As shown in figure 11, thermal conductance was highest among primates and the largest Glires, and was not associated with tradeoffs in organ mass (Figure 11A), but rather with a tradeoff between liver and brain *cMR*s (Figure 11B) that accompanied the general decrease in liver *cMR.80* and general increases in kidney, heart and brain *cMR.70*s (compare with Figure 10D).

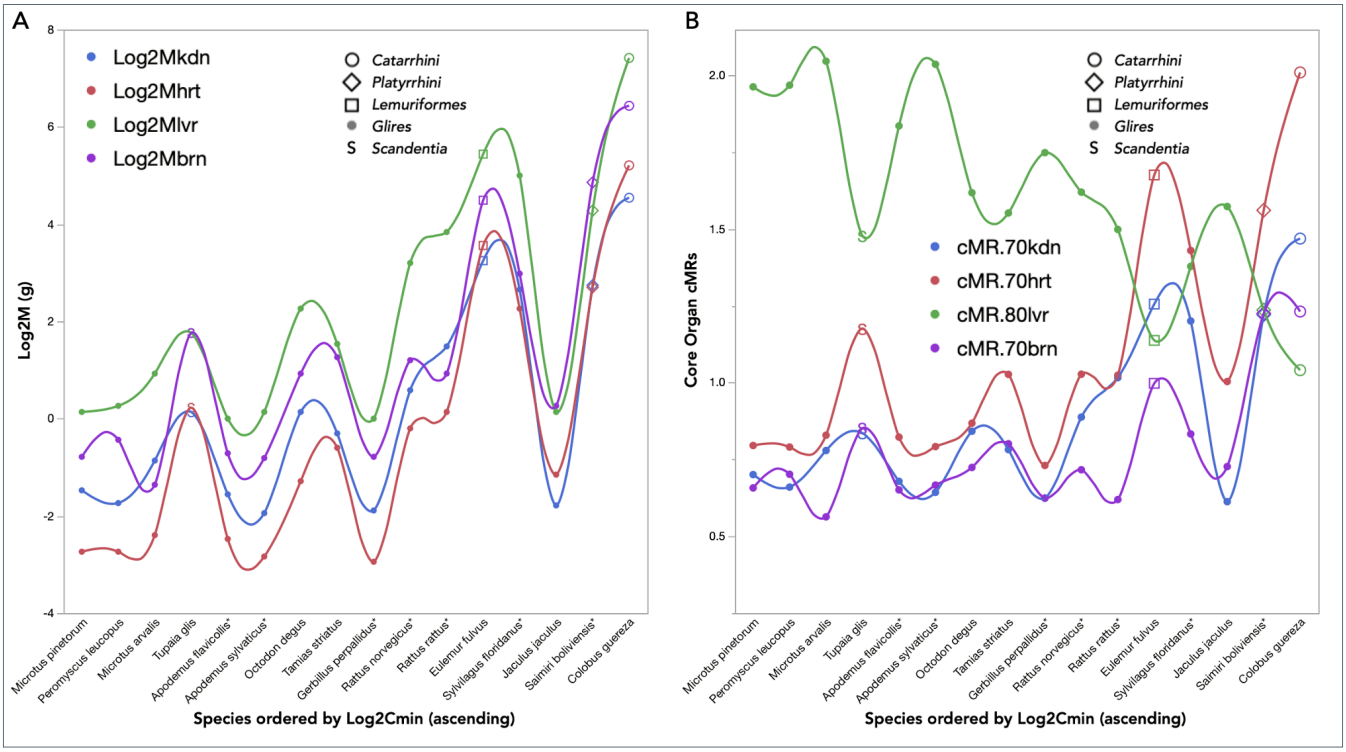

Figure 11. Thermal conductance covaries with a *cMR* tradeoff between liver and brain.
A. Like organ size, thermal conductance is a direct function of whole body size.
B. The size-related increase in thermal conductance is related to a compensatory tradeoff in core thermogenesis between brain and liver. Asterisks (*) represent species in the 4-organ dataset of Wang et al (2012) that were substituted for congeneric species in the C_{min} dataset of Khaliq et al (2014).

The evolution of tradeoffs of organ cMRs conforms to the core model of thermoregulation.

The evolutionary histories of the four organ *cMR*s provided compelling evidence that they have been constrained by their relationship to the core. We examined how the tradeoffs between brain and liver were related to the divergence of orders and species of Euarchontoglires, and to the corresponding changes in body size and number of microRNA families (Figure 12).

Opposite changes in direction of evolution were observed overall between body size and *cMR.80lvr*, and within each between Catarrhini and Glires (Figure 12). An accelerated increase in liver *cMR* accompanied the decrease in size of the two smallest of the Platyrrhini, one of which (*Callithrix pygmaea*) is a suspected heterotherm (Tattersall, 2012). All five of the smaller (< 1.0 kg) Platyrrhini exhibited elevated liver *cMR*s, consistent with adaptation to a low energy regime and increased reliance on gluconeogenesis, and among Glires, those species that underwent the greatest reductions in size also exhibited the highest increases in liver *cMR.80* (Figure 12).

Brain *cMR.70* accelerated and increased in intensity with the divergence of Haplorrhini, and again in the case of humans, in contrast to the relative stasis in Lemuriformes and Glires (Figure 12). Relative to the Platyrrhine ancestor, the five smallest species underwent an accelerated reduction in brain *cMR*, a clade-wide tradeoff that mirrored the tradeoff among Glires between liver and brain *cMR*s (Figure 12).

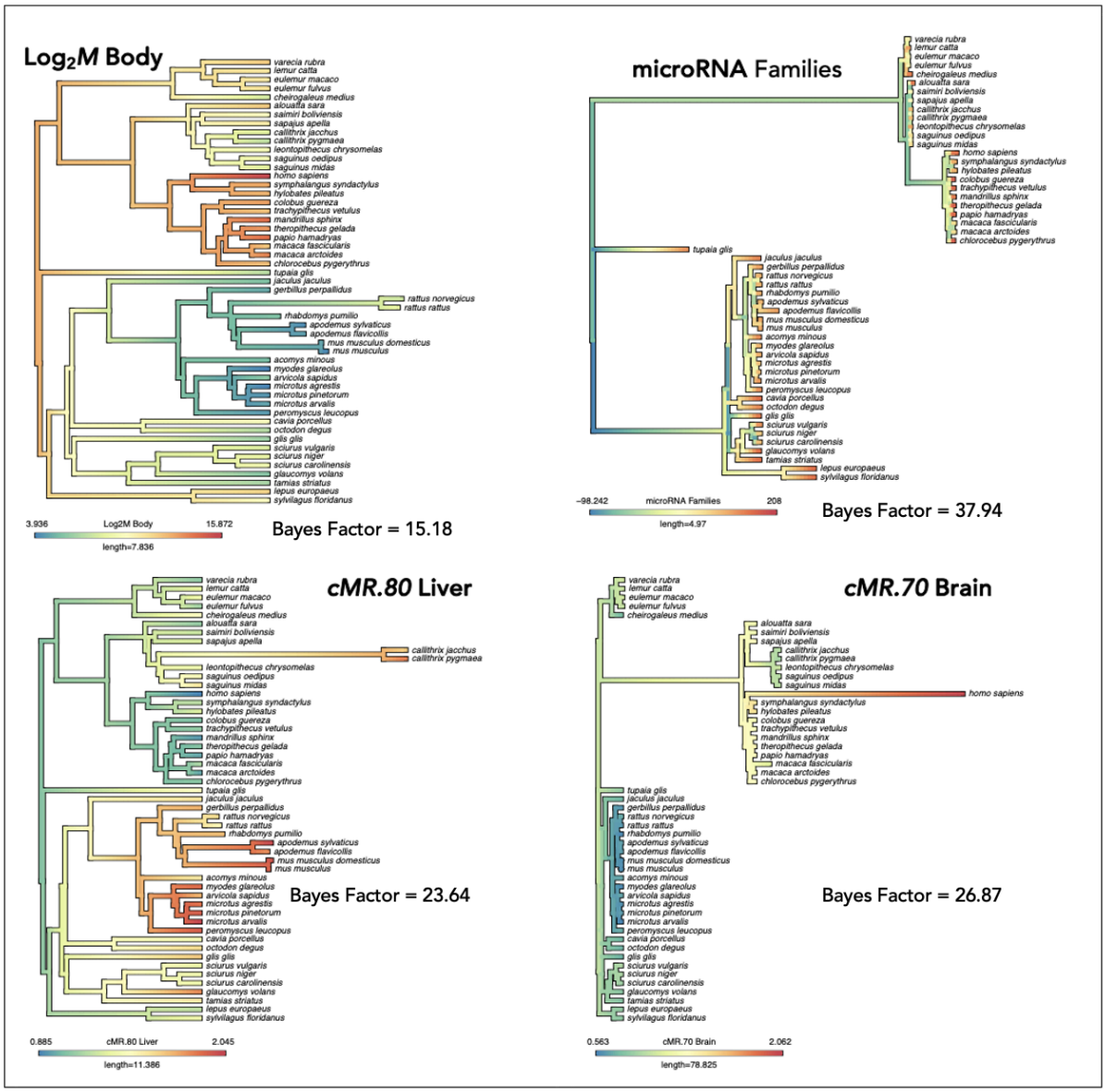

Figure 12. Variable rate phenograms of Log_2*Mbdy*, *mirFam*, *cMR.80lvr* and *cMR.70brn*. Bayes factors were computed from the difference between the median log likelihood (*Lh*) of the 1% most likely trees and the median *Lh* of the 1% of trees with the smallest non-zero sum of changes to branch length, *i.e.* those trees most similar to the reference time tree.

The evolution of *mirFam* recapitulated the divergence of the major clades of Euarchontoglires, with notable accelerations accompanying the divergence of the largest orders, Lagomorphs and Catarrhini (Figure 12); interestingly, these were mirrored by increases in intensity and evolutionary rate of *cMR.70hrt* (Figure 13). Relative kidney *cMR.70* levels generally resembled those of heart, with accelerated evolution in humans parallel to that of brain *sMR.70* (Figure 13), possibly signaling

adaptation to a diet enriched in protein and/or adaptation to an altered landscape of opportunities for hydration *versus* risks of dehydration.

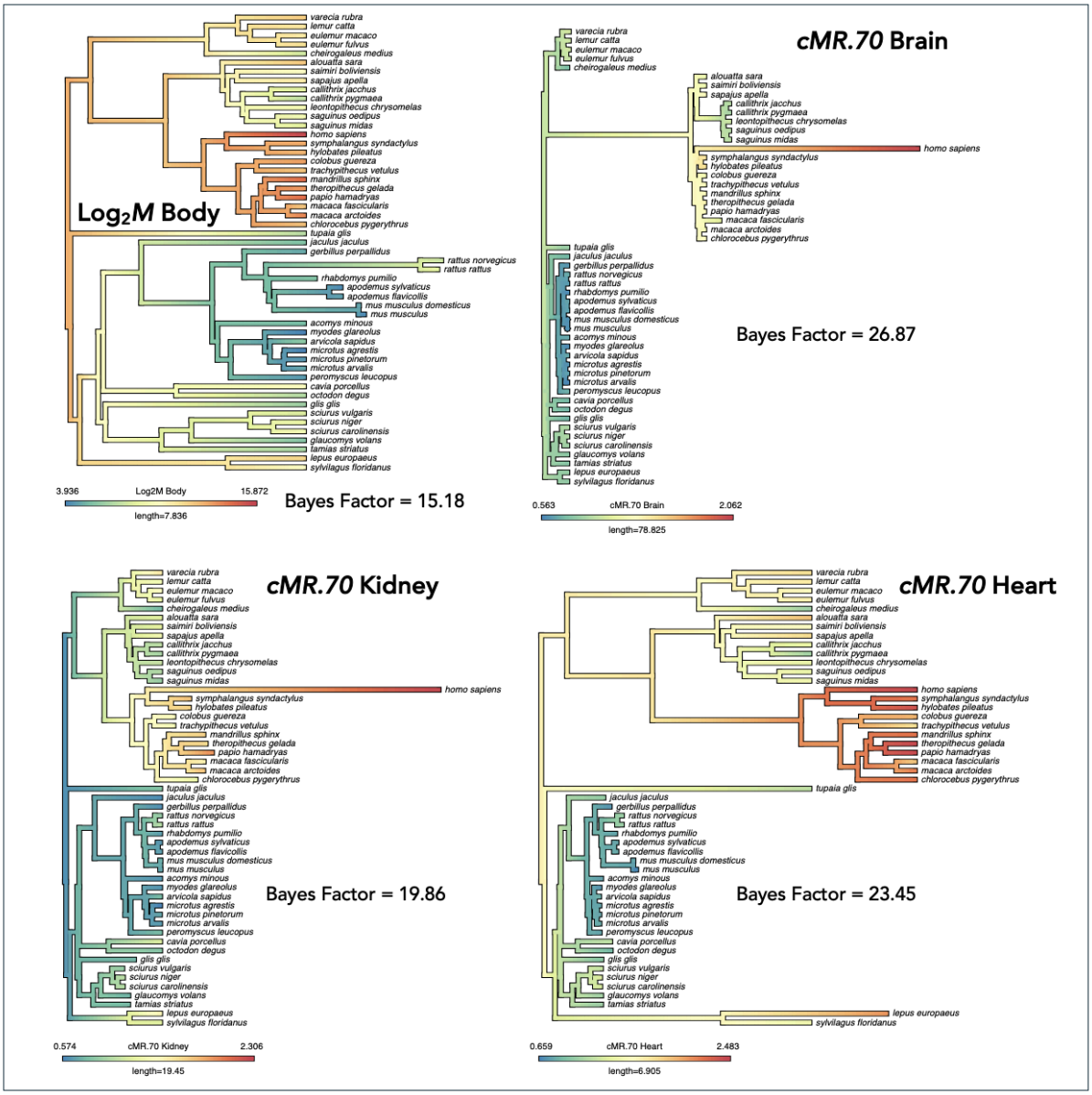

Figure 13. Variable rate phenograms comparing the evolution of kidney and heart *cMR*s to the evolution of body size.

SUMMARY AND CONCLUSIONS

Linearization of distributions of body mass and metabolic rate by log transformation has been *de rigueur* for phylogenetic comparative studies. Unlike log-derived *sMR*s, the c*MR*s of core thermogenic organs can be estimated according to physiological, thermodynamic and phylogenetic criteria. They can also be linearized with respect to the corresponding rate of thermogenesis of a four-organ core: only the latter method reveals the inverse relationship between brain and liver *cMR*s (Figure 14).

Countless comparative studies of whole body *rMR* in mammals have yielded *sMR* exponents ~ 0.75. Our analysis reveals that *cMR.75* corresponds approximately to the midpoints of the dynamic ranges of

the *mirFam* correlations with *cMRlvr*, *cMRbrn*, and *cMRbdy* (Figure 6). In other words, “Kleiber’s Law” for the log-based allometric scaling of mammalian *rMR* (Kleiber, 1934; Ballesteros et al, 2018) corresponds to the zone of weakest association between the core rate of thermogenesis and the global microRNA *milieu*, after controlling for body size.

The recent addition of hundreds of primate genome sequences (Kuderna et al, 2024) has been accompanied by ever more fine-grained studies of the covariance of traits suspected to influence the evolution of brain size. For the reasons elaborated in the Introduction, we submit that a fundamental assumption underlying these analyses – that log-transformed brain mass is an accurate index of brain energy expenditure – is not justified.

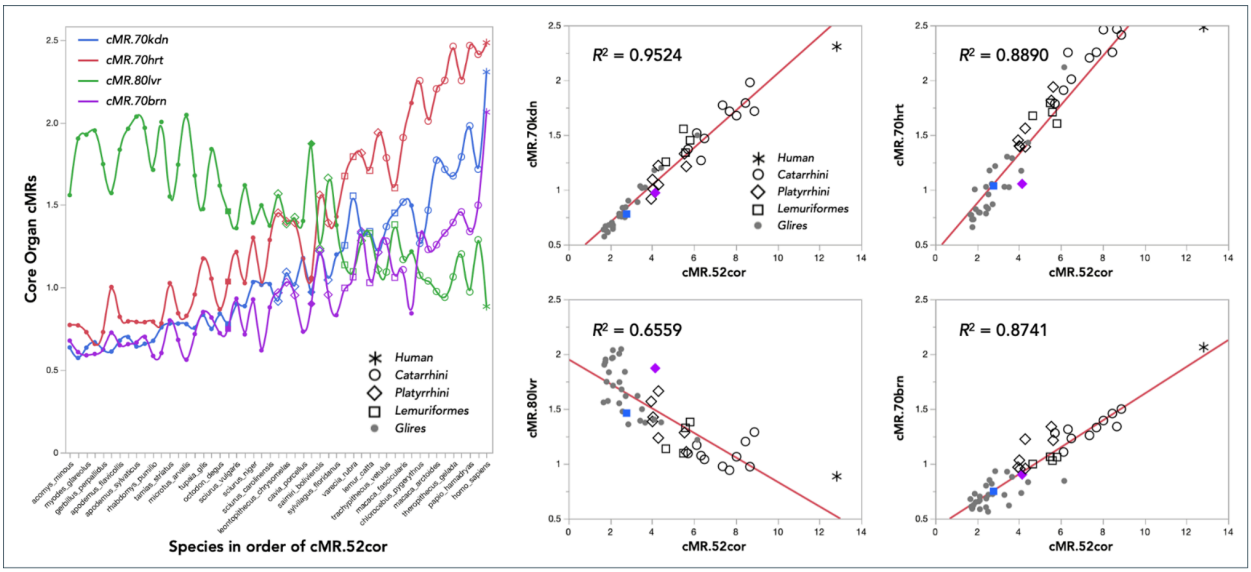

Figure 14. The thermodynamic origin of tradeoffs among core organ *cMR*s.
A. Species organ *cMR*s are proportional to the predicted species rate of core thermogenesis.
B. Linear regressions of individual organ *cMR*s on the *cMR* of the model thermogenic core.

Of the six possible tradeoffs in *cMR* among the four thermogenic organs, why is the brain-liver tradeoff the most significant? In a prolonged state of fasting, the liver is the primary organ of gluconeogenesis: the glucagon-dependent reduction of amino acid backbones fueled by free fatty acids released from adipose tissue. The oxidation of fatty acids also generates ketone bodies, which can supply up to 60% of the human brain’s energy supply during a prolonged fast, thereby sparing muscle protein (Owen et al, 1967; Garcia-Rodriguez and Giménez-Cassina, 2021). If an evolutionary increase in reliability of the energy supply meant a decrease in the frequency of fasting, hence reliance on gluconeogenesis and ketogenesis, then retention of the ancestral liver size and *cMR* would have been inefficient. Such a dynamic would have been reinforced if brain enlargement led to greater reliability of the energy supply.

We propose the following example of a *cMR*-based model of brain size evolution based on a simple feedback loop between brain size and the reliability of the energy supply: improvements in energy

reliability facilitate increases in brain size, which in turn favor further improvements in energy reliability, up to the limits imposed by anatomy and physiology *e.g.* the diameter of the birth canal and the physiological limit on the rate of heat dissipation (Speakman and Król, 2010). This neutral model reduces several current hypotheses (Expensive Brain/Ecological Brain/Cognitive Buffer) (Heldstab et al. 2022) to one that does not presuppose any underlying mechanism. It is a classic logistic model, with cMR_{max} standing in for carrying capacity in a population logistic model:

$$\mathbf{d(}\boldsymbol{cMRbdy}\mathbf{)\ /\ d(}\boldsymbol{Vbrn^*}\mathbf{) = }\boldsymbol{r} \bullet \boldsymbol{cMRbdy}\ \mathbf{[1 - (}\boldsymbol{cMRbdy}\ /\ \boldsymbol{cMRbdy_{max}}\mathbf{)],}$$

where ***Vbrn**** is the log ratio of endocranial volume to body mass, ***r*** represents the growth rate, and the range of ***cMRbdy*** has been scaled to 1.0.

We applied this model to the primate brain size dataset of Grabowski et al (2023), fitting it to *mirFam*, a proxy for *cMRbdy i.e.* the overall rate of energy utilization (Figure 15A). Unexpectedly, the model revealed that relative brain size is a predictor of *mirFam*, rather than *vice versa*, lending credence to the proposition that larger brains were associated with improvements in the reliability of the energy supply.

Given that the relative sizes of the three other thermogenic organs also fit logistic models for *mirFam* (Supplementary Figure S4), the question arises as to which relationship is the principal driver of adaptation. In phylogenetic regressions for organ *cMR*s ranging from *cMR*.60 - *cMR*.80, kidney, heart and liver *cMR*s varied independently of phylogeny (Pagel's *lambd*a = 0), while the variation of brain *cMR*.60 - *cMR*.80 with respect to *mirFam* was secondary to phylogenetic distance (Pagel's *lambda* = 1 in each case), suggesting that the divergence of primate species largely coincided with changes in the relationship of *mirFam* to brain mass and *cMR* (Supplementary Table S3) (Pagel, 1999).

Returning to the logistic model based on relative brain size, a variable rate phenogram for primate species was generated using the ratios from a Hubbert linearization of the logistic function (Figure 15B) (Hubbert, 1982). Thus, the color scale represents the rank on the logistic curve which, in general, tracks body size (compare with Figure 10A). The three smallest species, a Lemuriform and a pair of Callitrichinae, exhibited an accelerated rate of descent in rank. *Cheirogaleus medius* is a heterotherm, and *Callithrix pygmaea* may also be heterothermic (Tattersall, 2012), indicating that the baseline of the logistic function represents a regime of minimal energy reliability, perhaps related to low calorie-density folivory or insectivory.

Following this logic, we can ask what sort of constraint might be encountered near the plateau of this model? A likely candidate would be the physiological limit on the rate of heat dissipation (Speakman and Król, 2010; Fromm and Sorger, 2023). During exercise with progressive hyperthermia, human brain

temperature increases in parallel with that of the body core, leading to hyperthermia and fatigue (Nybo, 2012; Nybo and González-Alonso, 2015; Tsuji et al, 2016). Over a period spanning 700,000 years of human evolution, body mass and shape varied inversely with temperature, indicative of selection in response to thermoregulatory demands (Stibel, 2023).

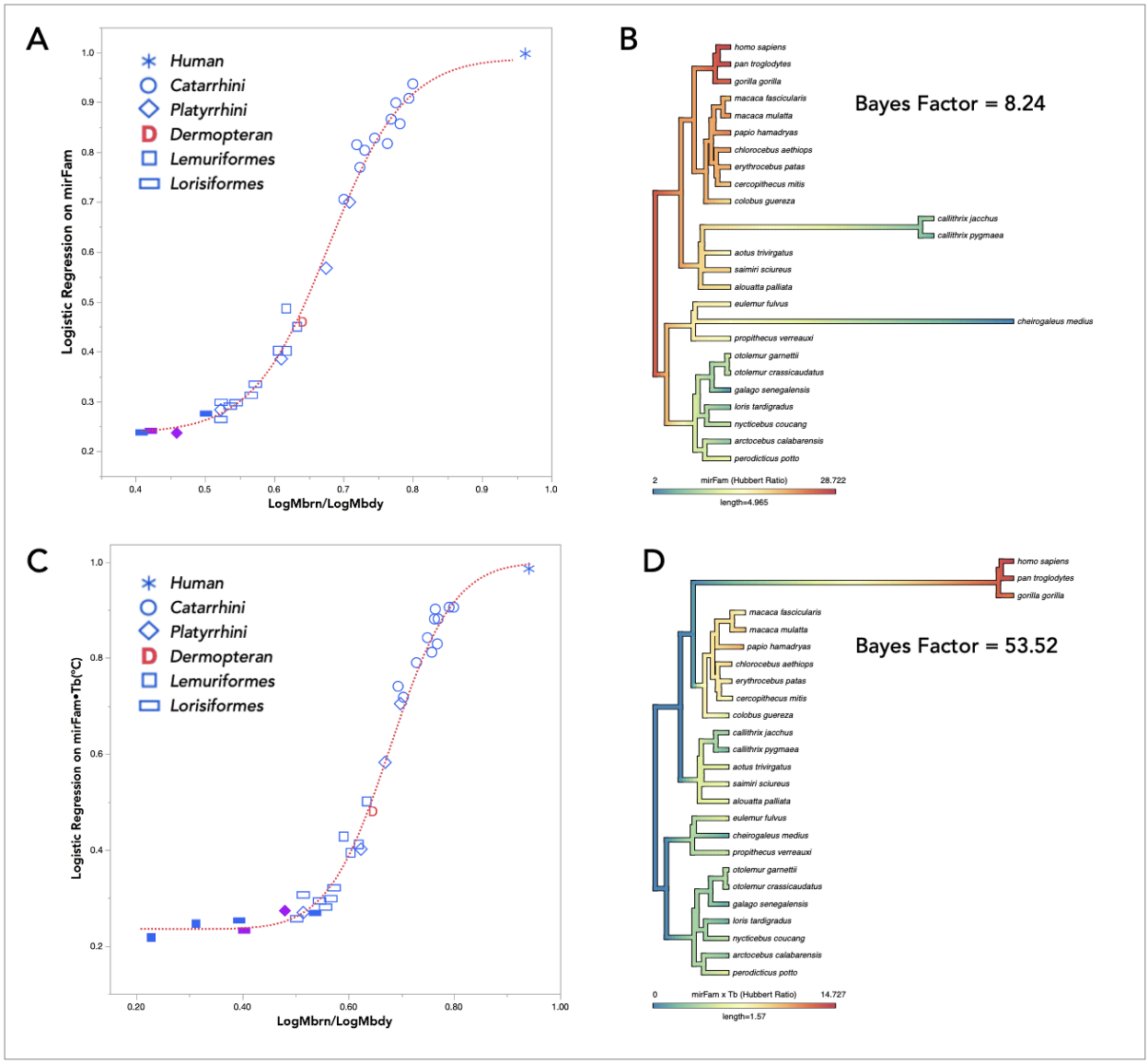

Figure 15. Logistic models of brain size evolution (data from Grabowski et al, 2023).
A, C. For these idealized models (R^2 = 1.00), *mirFam* or *mirFam*•T_b(ºC) was that predicted by the original logistic regression model (R^2 = 0.90 and 0.86, respectively) (jitter applied).
Filled symbols: heterotherms (blue), suspected heterotherms (purple). D = *Galeopterus variegatus*.
B, D. Variable rate phenograms of the Hubbert linearization of the logistic functions.

Previously we reported several observations indicating a reciprocal relationship in the evolution of body temperature and metabolic rate: in the case of primates, body temperatures (T_b) were inversely correlated with *mirFam* (Fromm and Sorger, 2023). This conserved nature of this relationship can be visualized by ranking primate species according to the product of *mirFam* x T_b (Supplementary Figure S6). We hypothesized that this product is representative of the heat dissipation limit: when ordered

according to the rate of core thermogenesis (*cMR.52cor*), *mirFam* x T_b tracks thermal conductance (Supplementary Figure S7). In this case, accelerated evolution near the plateau of a *mirFam* x T_b logistic model might signal a thermoregulatory adaptation. This appears to be have been the case for the divergence of hominid apes (Figure 15C, D) and accords well with the disproportionate increase in the total mass of the 4-organ core that accompanied the enlargement of the hominid brain (Figure 3), the leftward shift in the *mirFam* correlation profiles for brain and liver (Figure 5) and the associated variation in thermal conductance (Figure 11, Supplementary Figures S6 and S7).

Given that the brain is the only mammalian organ with its own exoskeleton, preventing outward heat transfer by diffusion or convection, the cerebrovascular circulation is the only available mechanism to maintain brain temperature homeostasis. Based on the the dimensions of the vascular foramina in extant and fossil apes, Seymour et al (2019) observed that the flow rates in the internal carotid arteries of extant chimpanzee, gorilla and orangutans were significantly higher than in those of 3 million year-old australopithecines with brains of equal or greater size, a mechanism that fits the interpretation of the *mirFam* x T_b phenogram as a thermoregulatory adaptation in the human lineage.

Bayesian inference predicts opposite evolutionary trends for the evolution of the relationship to brain size of *mirFam* and *mirFam* x T_b: descending in rank on the *mirFam* tree, and ascending in rank on the tree for *mirFam x* T_b (Figure 15). This model would assign the ancestral primate a high rank with respect to energy reliability and a low rank with respect to the heat dissipation limit, a propitious combination for the founder of a new order of mammals, perhaps situated in a new valley in the fitness landscape (Duran-Nebreda et al, 2024). As we have previously noted (Fromm and Sorger, 2023), reparametrization of rates of energy consumption in terms of *mirFam*-based *cMR*s reveals an unexpected degree of integration of microRNA complements into the energy economy of homeotherms, the basis of which remains to be explored.

METHODS

Physiological Data

The masses and *rMR*s of the four thermogenic organs were obtained from the dataset of Wang et al (2012), itself mainly derived from the compilation of Navarette et al (2011) (Supplementary Table S1). Values for thermal conductance (C_{min}) were obtained from the dataset of Khalig et al (2014). For comparison with core organ masses and cMRs, we substituted congeneric species from the dataset of Wang et al (2012). Where C_{min} was available for two or more species, we chose the one with the mass closest to the species in the Wang dataset.

MicroRNA Families

Complements of microRNA families were obtained from the most complete assembly for each species using covariance model MirMachine (Umu et al, 2023), trained on the manually-curated database MirGeneDB2.1 (Fromm et al 2021) (Supplementary Tables S1 and S2).

Phylogenetic Trees

Using Mesquite © (2021) we derived ultrametric trees for 51 Euarchontoglires or 25 primates from the phylogenies of Alvarez-Carretero et al (2021) and Shao et al (2023), respectively.

Variable Rate Phenograms

Variable rate trees and ancestral node values were inferred using BayesTraits.V4 (Pagel, 1999; Pagel et al, 2004; Venditti et al, 2011) (software available at www.evolution.rdg.ac.uk). Bayes factors for variable rate trees were computed from the difference between the median of the top 1% likelihoods and the median likelihood of the trees with lowest 1% sum of changes to branch length (Fromm and Sorger, 2023). Phenograms were generated using Phytools (Revell, 2012).

Statistics

Linear, partial least squares, and logistic regressions and normal mixture clustering were carried out and visualized using JMP16 ®. All R^2 values were adjusted for the number of predictors. Phylogenetic linear regressions were carried out using the R: CAPER package (Orme, 2013).

DATA AVAILABILITY

The original data with accompanying references and the results of all analyses referred to in the text are provided in the Supplementary Information (below).

ACKNOWLEDGMENT

BF is supported by the Tromsø forskningsstiftelse (TFS) [20_SG_BF 'MIRevolution'].

AUTHOR CONTRIBUTIONS

Conceptualization: TS; Methodology: TS; Investigation: BF and TS; Writing – Original Draft: TS; Writing – Review & Editing: BF and TS; Visualization: BF and TS; Funding Acquisition: BF.

DECLARATION OF INTERESTS The authors declare no competing interests.

REFERENCES

Aiello LC and Wheeler P. 1995. The expensive-tissue hypothesis: the brain and the digestive system in human and primate evolution. *Curr Anthro* 36: 199 - 221.

Álvarez-Carretero S, Tamuri A, Battini M, Nascimento F, Carlisle E, Asher R, Yang Z, Donoghue P and Dos Reis M. 2022. A species-level timeline of mammal evolution integrating phylogenomic data. *Nature* 602: 263 - 267.

Ballesteros FJ, Martinez VJ, Luque B, Lacasa L, Valor E and Moya A. 2018. On the thermodynamic origin of metabolic scaling. *Scientific Reports* 8: 1448.

Bennett JM, Sunday J, Calosi P, Villalobos F, Martínez B, Molina-Venegas R, Araújo MB, Algar AC, Clusella-Trulas S, Hawkins BA, Keith SA, Kühn I, Rahbek C, Rodríguez L, Singer A, Morales-Castilla I and Olalla-Tárraga MA. 2021. The evolution of critical thermal limits of life on Earth. *Nature Comms* 12: 1198 (1-9).

Buttgereit F and Brand MD. 1995. A hierarchy of ATP-consuming processes in mammalian cells. *Biochem J* 312: 163 -167.

Celeux G and Govaert G. 1995. Gaussian Parsimonious Clustering Models. *Pattern Recognition* 28: 781 - 793.

de Jong (1993). SIMPLS: An alternative approach to partial least squares regression. *Chemometrics and Intelligent Laboratory Systems*, 18: 251 - 263.

Deline B, Greenwood JM, Clark JW, Puttick MN, Peterson KJ, Donoghue PCJ. 2018. Evolution of metazoan morphological disparity. *PNAS* 29: E8909 - E8918.

Dempster AP, Laird NM and Rubin DB. 1977. Maximum Likelihood from Incomplete Data via the EM Algorithm. *J Roy Stat Soc B* 39: 1 - 38.

Elia M. Organ and tissue contribution to metabolic rate. 1992. In: Kinney JM, Tucker HN (eds), Energy metabolism: tissue determinants and cellular corollaries. pp 61 - 80. (Raven Press, NY).

Felsenstein J. 1985. Phylogenies and the comparative method. *Amer Naturalist* 125: 1 - 15.

Fonseca-Azevedo K and Herculano-Houzel S. 2012. Metabolic constraint imposes a tradeoff between body size and number of brain neurons in human evolution. *PNAS* 109: 18571 - 18576.

Fristoe TS, Burger JR, Balk MA, Khaliq I, Hof C and Brown JH. 2015. Metabolic heat production and thermal conductance are mass-independent adaptations to thermal environment in birds and mammals. *PNAS* 112: 15934 - 15939.

Fromm B, Høye E, Domanska D, Zhong X, Aparicio-Puerta E, Ovchinnikov V, Umu SU, Chabot, PJ, Kang W, Aslanzadeh M, Tarbier M, Mármol-Sánchez E, Urgese G, Johansen M, Hovig E, Hackenberg M, Friedländer MR and Peterson KJ. 2021. MirGeneDB 2.1: toward a complete sampling of all major animal phyla. *Nucl Acids Res* 50: D204 - D210.

Fromm B and Sorger T. 2023. Rapid adaptation of cellular metabolic rate to the microRNA complements of mammals and its relevance to the evolution of endothermy. *iScience*: 108740.

Garcia-Rodriguez D and Giménez-Cassina A. 2021. Ketone bodies in the brain beyond fuel metabolism: from excitability to gene expression and cell signaling. *Front Mol Neurosci* 14: 732120.

Grabowski M, Kopperud BT, Tsuboi M and Hansen TF. 2023. Both diet and sociality affect primate brain-size evolution. *Syst Biol* 72: 404 - 418.

Hansen TF. 1997. Stabilizing selection and the comparative analysis of adaptation. *Evolution* 51: 1341 - 1351.

Heldstab SA, Isler K, Graber SM, Schuppli C and van Schaik. 2022. The economics of brain size evolution in vertebrates. *Curr Biol* 32: R697 – R708.

Hubbert MK. 1982. Techniques of prediction as applied to the production of oil and gas. In Gass, Saul I. (ed.). Oil and Gas Supply Modeling (proceedings of a symposium held at the Department of Commerce, Washington, DC, June 18–20, 1980). NBS Special Publication 631. Washington (DC): National Bureau of Standards. pp. 16–141.

Isler K and van Schaik CP. 2012. Allomaternal care, life history and brain size evolution in mammals. *J Human Evol* 63: 52 - 63.

Isler K and van Schaik CP. 2014. How humans evolved large brains: comparative evidence. *Evol Anthropol* 23: 65-75.

Khaliq I, Hof C, Prinzinger R, Böhning-Gaese K and Pfenninger M. 2014. Global variation in thermal tolerances and vulnerability of endotherms to climate change. *Proc Roy Soc B* 281: 20141097 (1 - 8).

Kiyatkin AE. 2007. Brain temperature fluctuations during physiological and pathological conditions. *Eur J Appl Physiol* 101: 3 - 17.

Kleiber M. 1932. Body size and metabolism. *Hilgardia* 6: 315 - 353.

Koteja P. 2000. Energy assimilation, parental care and the evolution of endothermy. *Proc Roy Soc B* 267: 479 - 484.

Kuderna LFK, Gao H, Janiak MC . . . Bonet TM. 2023. A global catalog of whole-genome diversity from 233 primate species. *Science* 380: 9 - 60913.

Kummitha CM, Kalhan SC, Saidel GM and Lai N. 2014. Relating tissue/organ energy expenditure to metabolic fluxes in mouse and human: experimental data integrated with mathematical modeling. *Physiol Rep* e12159 (1 - 20).

Kuzawa CW, Chugani HT, Grossman LI, Lipovich L, Muzik O, Hof PR, Wildman DE, Sherwood CC, Leonard WR and Lange N. 2014. *PNAS* 111: 13010 - 13015.

Lande R. 1979. Quantitative genetic analysis of multivariate evolution, applied to the brain: body size allometry. *Evolution* 33: 402 - 416.

Magalhães JP, Abidi Z, dos Santos GA . . . Ka Po To P. 2024. Human Ageing Genomic Resources: updates on key databases in ageing research. *Nucl Acids Res* 52: D900 - D908.

Mascia-Lees FE, Relethford JH and Sorger T. 1986. Perspectives on permanent breast enlargement in human females. *Amer Anthro* 88: 423 - 428.

Navarette A, van Schaik CP and Isler K. 2011. Energetics and the evolution of human brain size. *Nature* 480: 91 - 93.

Naya DE, Spangenberg L, Naya H and Bozinovic F. 2013. Thermal conductance and basal metabolic rate are part of a coordinated system for heat transfer regulation. *Proc Roy Soc B* 280: 20131629.

Nybo L. 2012. Brain temperature and exercise performance. *Exp Physiol* 97: 333 - 339.

Nybo L, Secher NH and Nielsen B. 2002. Inadequate heat release from the human brain during prolonged exercise with hyperthermia. *J Physiol* 545: 697 - 704.

Nybo L and González-Alonso J. 2015. Critical core temperature: a hypothesis too simplistic to explain hyperthermia-induced fatigue. *Scand J Med Sci Sports* 25: 4 - 5.

Orme D, Freckleton RP, Thomas GH and Petzoldt T. 2013. CAPER: comparative analyses of phylogenetics and evolution in R. *Methods Ecol and Evol* 3: 141 - 151.

Owen OE, Morgan AP, Kemp HG, Sullivan JM, Herrera MG and Cahill GF.1967. Brain metabolism during fasting. *J Clin Inv* 46: 1589 - 1595.

Pagel M. 1999. Inferring the historical patterns of biological evolution. *Nature* 401: 877 - 884.

Pagel M, Meade A and Barker D. 2004. Bayesian estimation of ancestral character states on phylogenies. *Syst Biol* 53: 673 - 684.

Pontzer H, Brown MH, Raichlen DA . . . Ross SR. 2016. Metabolic acceleration and the evolution of human brain size and life history. *Nature* 533: 390 - 393.

Porter WP and Kearney M. 2009. Size, shape, and thermal niche of endotherms. *PNAS* 106: 19666 - 19672.

Revell LJ. 2012. phytools: an R package for phylogenetic comparative biology (and other things). *Methods Ecol Evol* 3: 217 - 223.

Scholander PF, Hock F, Walters V, Johnson F and Irving L. 1950. Heat Regulation in Some Arctic and Tropical Mammals and Birds. *Biol Bull* 99: 237 - 258.

Seymour RS, Bosiocic V, Snelling EP, Chikezie PZ, Hu Q, Nelson TJ, Zipfel P and Miller CV. 2019. Cerebral blood flow rates in recent great apes are greater than in *Australopithecus* species that had equal or larger brains. *Proc Biol Sci* 286(1915): 20192208.

Shao Y, Zhou, Li F . . . Wu DD. 2023. Phylogenomic analyses provide insights into primate evolution. *Science* 380: 913 - 924.

Simmen B, Pasquet P, Masi S, Koppert GJA, Wells JCK and Hladik CM. 2017. Primate energy input and the evolutionary transition to energy-dense diets in humans. *Proc Roy Soc B* 284: 20170577.

Smaers JB, Rothman RS, Hudson DR, Balanoff AM, Beatty B, Dechmann DKN, deVries D, Dunn, JC, Fleagle JG, Gilbert CC, Goswami A, Iwaniuk AN, Jungers WL, Kerney M, Ksepka DT, Manger PR, Mongle CS, Rohlf FJ, Smith NA, Soligo C, Weisbecker V and Safi K. 2021.
The evolution of mammalian brain size. *Sci Adv* 7: eabe2101 (1 - 11).

Speakman JR and Król E. 2010. Maximal heat dissipation capacity and hyperthermia risk: neglected key factors in the ecology of endotherms. *J Anim Ecol* 79: 726 – 746.

Stibel JM. 2023. Climate change is predictive of body size and proportionality in humans.
Evol Biol 50: 461 - 475.

Svensson EI, Arnold SJ, Bürger R et al. 2021. Correlational selection in the age of genomics.
Nat Ecol Evol 5, 562–573.

Tattersall GJ. 2012. Diurnal changes in metabolic rate in pygmy marmosets: Implications for sleep, torpor, and basal metabolism in primates. In: Ruf, T., Bieber, C., Arnold, W., Millesi, E. (eds)
Living in a Seasonal World, chapter 41: 471 - 480. Springer.

Tsuji B, Hayashi K, Kondo N and Nishiyasu T. 2016. Characteristics of hyperthermia-induced hyperventilation in humans. *Temperature* 3: 146 - 160.

Umu SU, Paynter VM, Trondsøn H, Buschmann T, Rounge TB, Peterson KJ and Fromm B. 2023. Accurate microRNA annotation of animal genomes using trained covariance models of curated microRNA complements in MirMachine. *Cell Genomics* 3: 100348.

Venditti C, Meade A. and Pagel M. 2011. Multiple routes to mammalian diversity.
Nature, 479, 393 - 396.

Walter GM and McCuigan K. 2023. Phenotypic evolution: predicting the future. *eLife* 12: e91450 (1 - 3).

Wang H, Wang B, Normoyle K, Jackson K, Spitler K, Sharrock MF, Miller CM, Best C, Llano D and Du R. 2014. Brain temperature and its fundamental properties: a review for clinical neuroscientists.
Front Neurosci 307: 1 - 17.

Wang ZM, Zhang J, Ying Z and Heymsfield SB. 2012. Organ-tissue level model of resting energy expenditure across mammals: new insights into Kleiber's Law. *ISRN Zool*: 673050 (1 - 9).

Yu Y, Hill AP and McCormick DA. 2012. Warm Body Temperature Facilitates Energy Efficient Cortical Action Potentials. *PLoS Comp Biol* e1002456: 1 - 16.

SUPPLEMENTARY INFORMATION

Clade	Wang Taxon Names	Names on Phylogeny	*mirFam*	*Mkdn* (g)	*Mhrt* (g)	*Mlvr* (g)	*Mbrn* (g)	*Mcor* (g)	*Mbdy* (g)	*MRkdn* (W)	*MRhrt* (W)	*MRlvr* (W)	*MRbrn* (W)	*MRcor* (W)	*MRbdy* (W)
Primates	*Alouatta sara*	*Alouatta palliata*	174	9.9	24	81.2	56.5	171.6	4399.6	13.7088	13.6112	33.6452	12.9948	73.96	169.5872
Primates		*Callithrix jacchus*	172	2.9	2.8	17.8	7.3	30.8	311.8	6.039	17.928	37.352	20.453	81.772	180.7072
Primates	*Cebualla pygmaea*	*Callithrix pygmaea*	171	1.9	0.86	13.5	4.4	20.66	162.66	6.8432	11.1622	29.0377	20.9296	67.9727	112.3625
Primates		*Cheirogaleus medius*	176	1	0.93	6.3	2.8	11.03	231.03	1.5238	0.94858	15.012	2.5432	20.02758	25.77858
Primates		*Chlorocebus pygerythrus*	199	12.1	42.6	89	80.8	224.5	5300.5	2.204	2.8616	16.643	3.8471	25.5557	35.7841
Primates		*Colobus guereza*	198	23.3	37	171	86.5	317.8	9749.8	2.9356	3.5644	14.553	6.2832	27.3362	46.7808
Primates		*Eulemur fulvus*	180	9.5	11.8	43.4	22.5	87.2	2500.2	1.4364	3.3495	13.248	4.0794	22.1133	33.0213
Primates		*Eulemur macaco*	180	14.2	9.1	77.8	24.2	125.3	1875.3	2.2227	3.4817	16.2184	4.78	26.7028	45.6892
Primates	Human	*Homo sapiens*	208	250	320	1700	1300	3570	59970	9.2862	14.1312	40.05	25.56	89.0274	199.0161
Primates	*Hylobates concolor*	*Hylobates pileatus*	195	35.2	58.2	293	137.8	524.2	6550.2	13.3043	25.16	63.612	27.9395	130.0158	323.3718
Primates		*Lemur catta*	178	11.2	11.7	72.9	22.8	118.6	2074.6	12.789	17.135	50.27	15.162	95.356	195.6392
Primates		*Leontopithecus chrysomelas*	173	4.1	3.8	18.9	13.2	40	642	27.4	39.162	78.566	35.518	180.646	471.706
Primates	*Macaca nigra*	*Macaca arctoides*	205	50	61	241	118	470	15870	42.6393	63.242	115.64	49.59	271.1113	669.3613
Primates	Monkey	*Macaca fascicularis*	207	21	23	110	42	196	4500	21.394	51.5696	84.252	44.5244	201.74	419.94
Primates		*Mandrillus sphinx*	194	49.9	76	331	168	624.9	23024.9	0.8932	1.31274	3.9304	2.006	8.14234	13.62034
Primates		*Papio hamadryas*	197	80.3	103	392	174	749.3	23249.3	2.229	2.4725	9.2769	3.8025	17.7809	31.2792
Primates	*Saguinus lagonotus*	*Saguinus midas*	170	1.9	3.3	14.4	7.8	27.4	330.4	0.2841	0.2094	2.2764	0.56832	3.33822	4.47022
Primates		*Saguinus oedipus*	172	3.1	3.7	20.9	10	37.7	623.7	0.23424	0.1456	1.39829	0.2828	2.06093	2.90093
Primates		*Saimiri boliviensis*	174	6.7	6.5	19.4	29	61.6	1002.6	0.609	0.34636	3.7466	0.7304	5.43236	8.15126
Primates		*Sapajus apella*	171	10.4	13.4	49.3	50.8	123.9	1749.9	0.5126	0.25916	3.4181	0.29133	4.48119	5.79399
Primates		*Symphalangus syndactylus*	194	43.7	51.5	294	143	532.2	8500.2	1.179	0.93177	9.5588	1.2834	12.95297	20.57737
Primates		*Theropithecus gelada*	203	38	77.2	236	140.9	492.1	11402.1	0.27412	0.10241	1.43344	0.29232	2.10229	2.94789
Primates		*Trachypithecus vetulus*	197	15.4	19.2	90	72	196.6	4999.6	0.47379	0.21728	3.2058	0.3715	4.26837	5.62837
Primates		*Varecia rubra*	181	22.4	18.1	72.2	35.7	148.4	4200.4	0.25038	0.19992	2.1967	0.44973	3.09673	4.03113
Scandentia		*Tupaia glis*	151	1.1	1.17	3.4	3.4	9.07	141.07	0.31892	0.24768	1.835	0.46055	2.86215	4.13635
Glires		*Acomys minous*	157	0.32	0.18	0.9	0.9	2.3	42.3	0.779	0.98487	6.3756	1.54	9.67947	18.10547
Glires		*Apodemus flavicollis*	141	0.34	0.18	1	0.61	2.13	25.13	7.2688	9.5589	41.0427	9.1884	67.0588	118.8928
Glires		*Apodemus sylvaticus*	155	0.26	0.14	1.1	0.57	2.07	18.07	6.0705	9.4282	23.219	8.82	47.5377	109.5518
Glires		*Arvicola sapidus*	149	0.7	0.28	2.6	1.1	4.68	61.68	9.301	7.5257	44.9684	9.8736	71.6687	118.9187
Glires	Guinea Pig	*Cavia porcellus*	174	5.6	2.3	27	4.7	39.6	799.6	4.623	5.785	13.2502	12.934	36.5922	64.7281
Glires		*Gerbillus perpallidus*	147	0.27	0.13	1	0.58	1.98	29.98	110	140.8	340	312	902.8	1489.36
Glires		*Glaucomys volans*	176	0.59	0.56	2.9	1.9	5.95	54.95	20.768	41.4966	121.302	47.1276	230.6942	362.6636
Glires		*Glis glis*	168	0.68	0.48	3.2	1.5	5.86	83.86	25.2149	35.5865	113.484	47.047	221.3324	388.6604
Glires		*Jaculus jaculus*	158	0.29	0.45	1.1	1.2	3.04	48.04	7.26	31.1406	38.982	28.4416	105.8242	221.0494
Glires		*Lepus europaeus*	173	18.5	28.9	90.4	14.8	152.6	3338.6	26.4969	46.74	97.645	48.048	218.9299	617.6499
Glires		*Microtus agrestis*	148	0.17	0.12	0.63	0.39	1.31	15.31	11.544	22.3108	44.748	5.5648	84.1676	162.2246
Glires		*Microtus arvalis*	153	0.55	0.19	1.9	0.39	3.03	27.03	4.3533	4.2864	22.048	3.5392	34.2269	61.949
Glires		*Microtus pinetorum*	154	0.36	0.15	1.1	0.58	2.19	21.19	0.57664	0.57312	4.256	0.954	6.35976	9.89316
Glires		*Mus musculus*	167	0.28	0.07	0.68	0.36	1.39	15.39	0.67473	0.76758	3.6366	1.4784	6.55731	10.79621
Glires	Mouse	*Mus musculus domesticus*	167	0.51	0.16	1.8	0.5	2.97	27.97	0.51802	0.70224	4.3094	1.2825	6.81216	9.19356
Glires		*Myodes glareolus*	143	0.24	0.1	0.67	0.35	1.36	15.36	1.3056	1.7629	5.3185	3.3831	11.7701	21.4049
Glires		*Octodon degus*	156	1.1	0.41	4.8	1.9	8.21	129.21	2.304	2.6488	12.8904	3.6075	21.4507	39.9589
Glires		*Peromyscus leucopus*	160	0.3	0.15	1.2	0.74	2.39	22.39	0.8998	0.46494	5.6736	1.1343	8.17264	13.26674
Glires		*Rattus norvegicus*	168	1.5	0.87	9.2	2.3	13.87	209.87	3.9368	2.1022	19.602	2.1667	27.8077	51.4437
Glires	Rat	*Rattus rattus*	167	2.8	1.1	14.3	1.9	20.1	390.1	0.25752	0.57375	1.6973	0.8256	3.35417	5.59067
Glires		*Rhabdomys pumilio*	161	0.41	0.21	1.8	0.6	3.02	50.02	0.28704	0.23274	1.4337	0.63	2.58348	4.61148
Glires		*Sciurus carolinensis*	175	3.2	2.8	16.4	7.5	29.9	595.9	0.34272	0.21075	2.1175	0.44892	3.11989	4.20479
Glires		*Sciurus niger*	165	3	2.5	10.7	7.5	23.7	412.7	0.16592	0.17472	1.31481	0.31512	1.97057	2.81057
Glires		*Sciurus vulgaris*	175	1.7	1.7	5.5	6.3	15.2	274.2	0.24948	0.17511	1.748	0.4263	2.59889	4.10249
Glires		*Sylvilagus floridanus*	170	6.3	4.8	32	7.9	51	972	2.0888	1.0945	12.584	0.9709	16.7382	29.7252
Glires		*Tamias striatus*	173	0.81	0.66	2.9	2.4	6.77	103.77	0.36285	0.26607	2.7414	0.4098	3.78012	6.09722

Table S1. Summary of species *mirFam*, mass and resting metabolic rates for organs, core and body. All physiological data were obtained from Wang et al (2012), most of which were compiled by Navarette et al (2011). The names of the indicated taxa were substituted with congeneric species on the phylogenies of Álvarez-Carretero et al (2022) and Shao et al (2023).

Order	Species	*mirFam*	ECV	Mass (g)	T_b (°C)
Catarrhini	*Homo sapiens*	208	1252.00	50000	37.0
Catarrhini	*Pan troglodytes*	206	368.35	44967	35.7
Catarrhini	*Gorilla gorilla*	202	490.41	120950	35.5
Catarrhini	*Macaca fascicularis*	207	63.98	4251	37.6
Catarrhini	*Macaca mulatta*	208	88.98	6793	37.3
Catarrhini	*Papio hamadryas*	197	146.17	14150	38.0
Catarrhini	*Chlorocebus aethiops*	199	65.00	3720	36.8
Catarrhini	*Erythrocebus patas*	201	97.73	9450	39.3
Catarrhini	*Cercopithecus mitis*	200	71.33	6109	37.5
Catarrhini	*Colobus guereza*	198	74.39	8589	37.0
Platyrrhini	*Callithrix jacchus*	172	7.24	320	36.0
Platyrrhini	*Callithrix pygmaea*	171	4.17	116	35.2
Platyrrhini	*Aotus trivirgatus*	177	16.85	989	38.0
Platyrrhini	*Saimiri sciureus*	174	24.14	799	38.0
Platyrrhini	*Alouata palliata*	174	49.88	6250	36.0
Lemuriformes	*Eulemur fulvus*	180	25.77	2292	36.5
Lemuriformes	*Cheirogaleus medius*	176	2.60	140	38.0
Lemuriformes	*Propithecus verreauxi*	180	26.21	2955	36.0
Lorisiformes	*Otolemur garnettii*	166	11.50	764	36.0
Lorisiformes	*Otolemur crassicaudatus*	166	11.78	1150	36.6
Lorisiformes	*Galago senegalensis*	165	3.96	194	37.9
Lorisiformes	*Loris tardigradus*	166	5.87	193	35.5
Lorisiformes	*Nycticebus coucang*	167	10.13	653	35.4
Lorisiformes	*Arctocebus calabarensis*	166	6.92	309	36.0
Lorisiformes	*Perodicticus potto*	169	12.42	835	35.4

Table S2. Summary of *mirFam*, brain volume (ECV), body mass and temperature for 25 primates. Endocranial volume (ECV) and body mass were obtained from Grabowski et al, 2023. Body emperatures were obtained from the AnAge database (Magalhães et al, 2024).

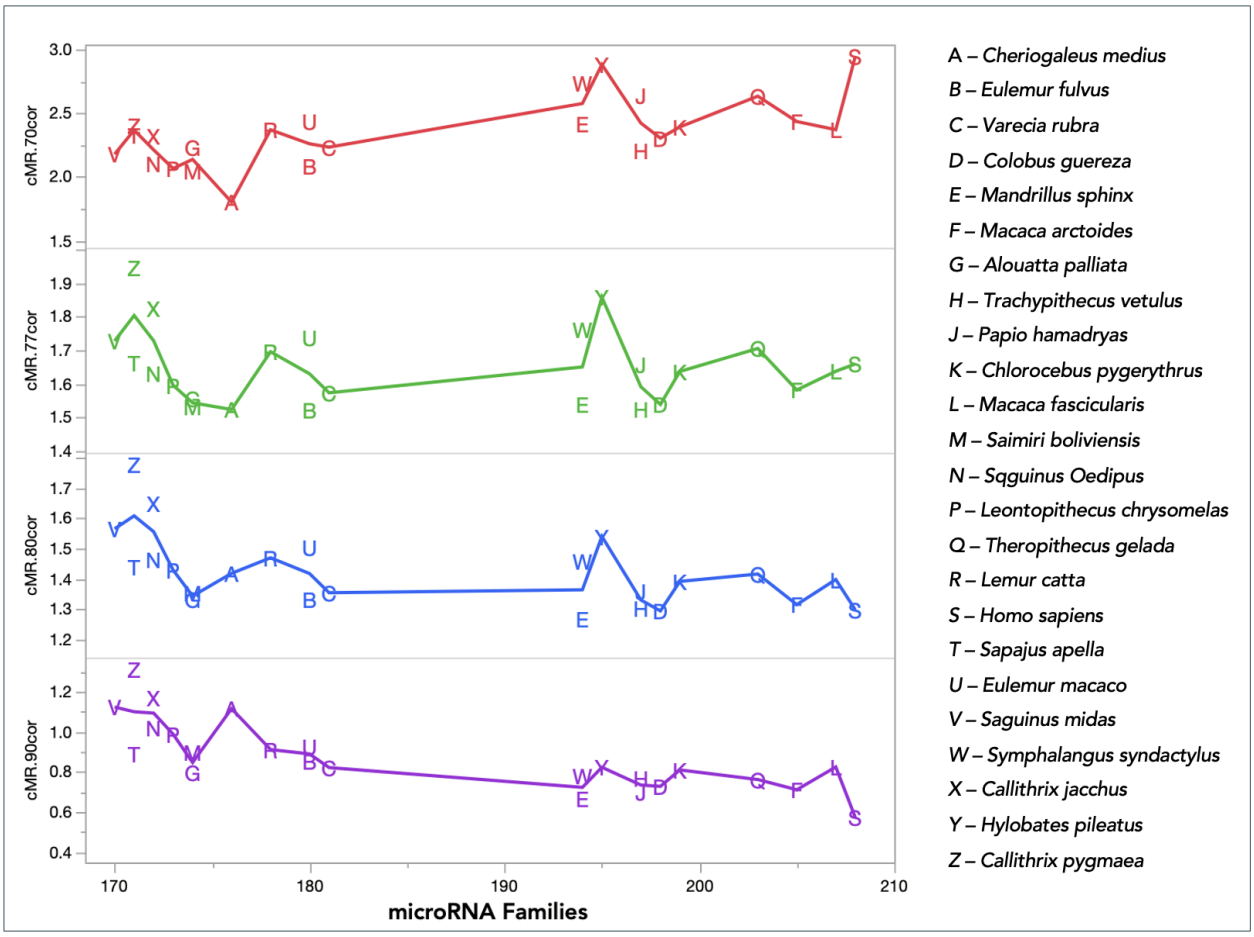

Figure S1. Cellular *MR*s determine the species rank of *cMR*/*mirFam* ratios. Primate species were labeled in order of magnitude of *cMR.75*/*mirFam*, and their distributions plotted as *cMR* was varied. Note the changes in rank order in addition to the changes in overall slope.

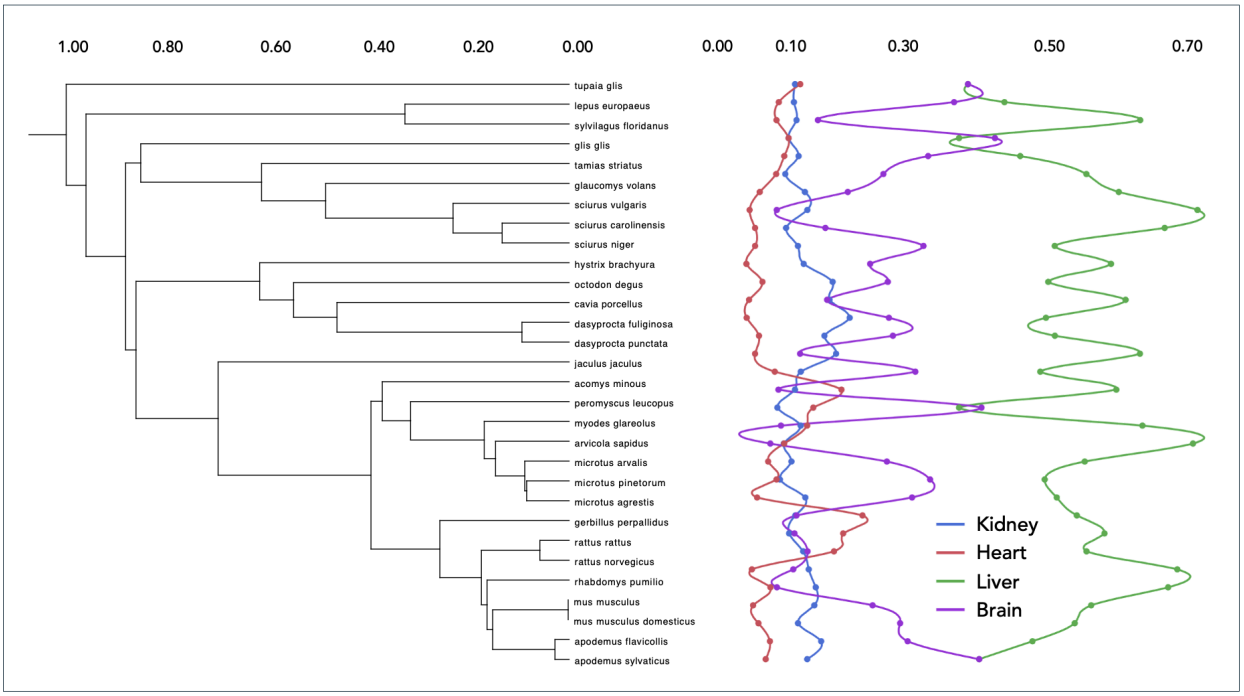

Figure S2. The proportions of brain and liver vary reciprocally in the Euarchontoglires 4-organ core. Species include one Scandentia, two Lagomorpha, and 27 Glires, including three Sciuridae.

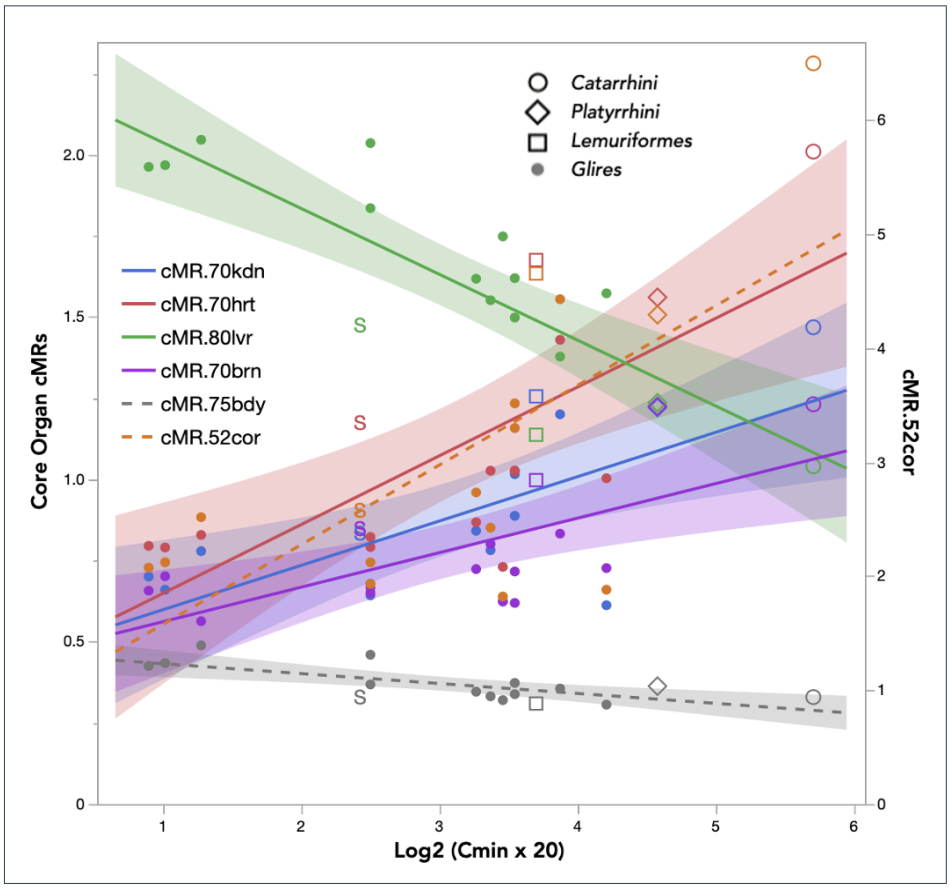

Figure S3. Variation of core organ *cMR*s with respect to thermal conductance ($Log_2 C_{min}$). C_{min} values for a subset of 16 Euarchontoglires were obtained from Khaliq et al (2014). Compare with Figure 6 in the main text.

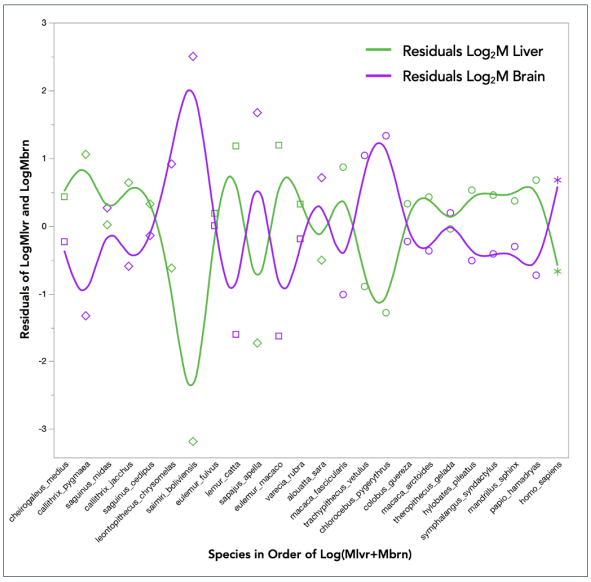

Figure S4. Tradeoffs between liver and brain as a function of their combined mass. The "phase shift" between the residuals of liver and brain with respect to the core (Figure 10D) can be isolated by repeating the regression with respect to Log (*Mlvr* + *Mbrn*), demonstrating that the periodicity depends on autocorrelation.

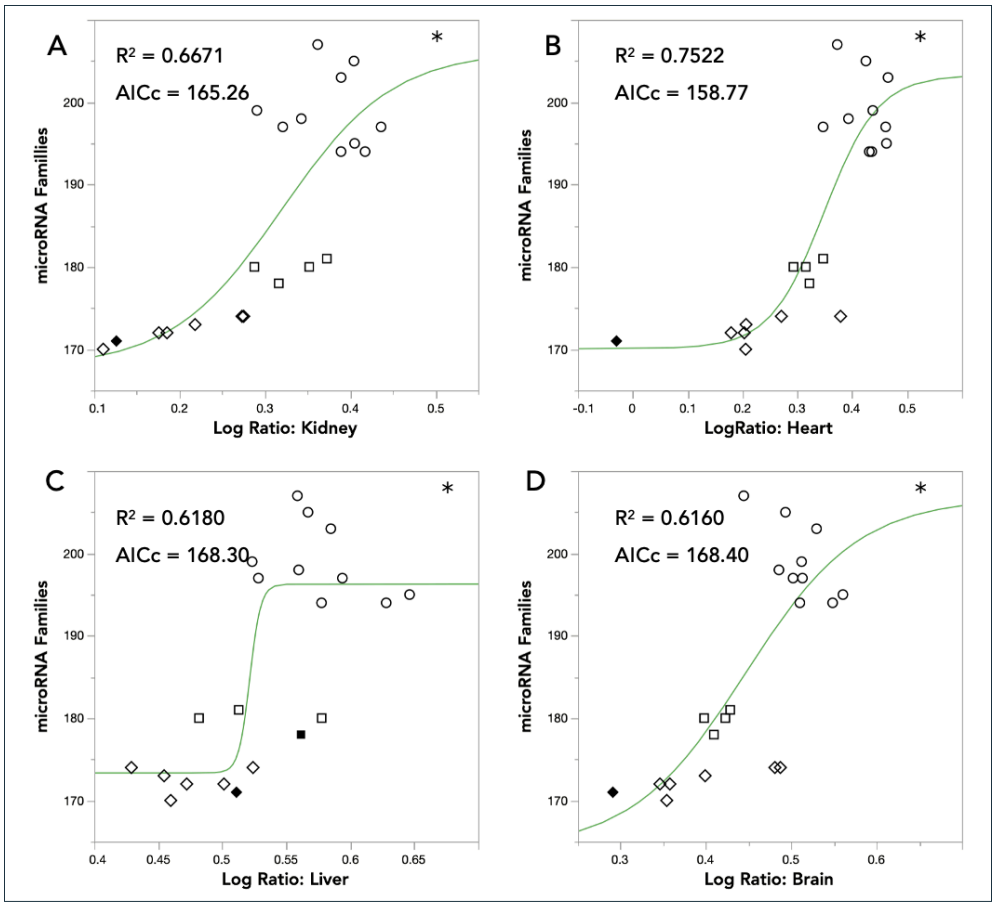

Figure S5. Logistic models for the size evolution of four thermogenic organs.
Symbols representing clades as in previous figures, with filled symbols representing heterotherms.

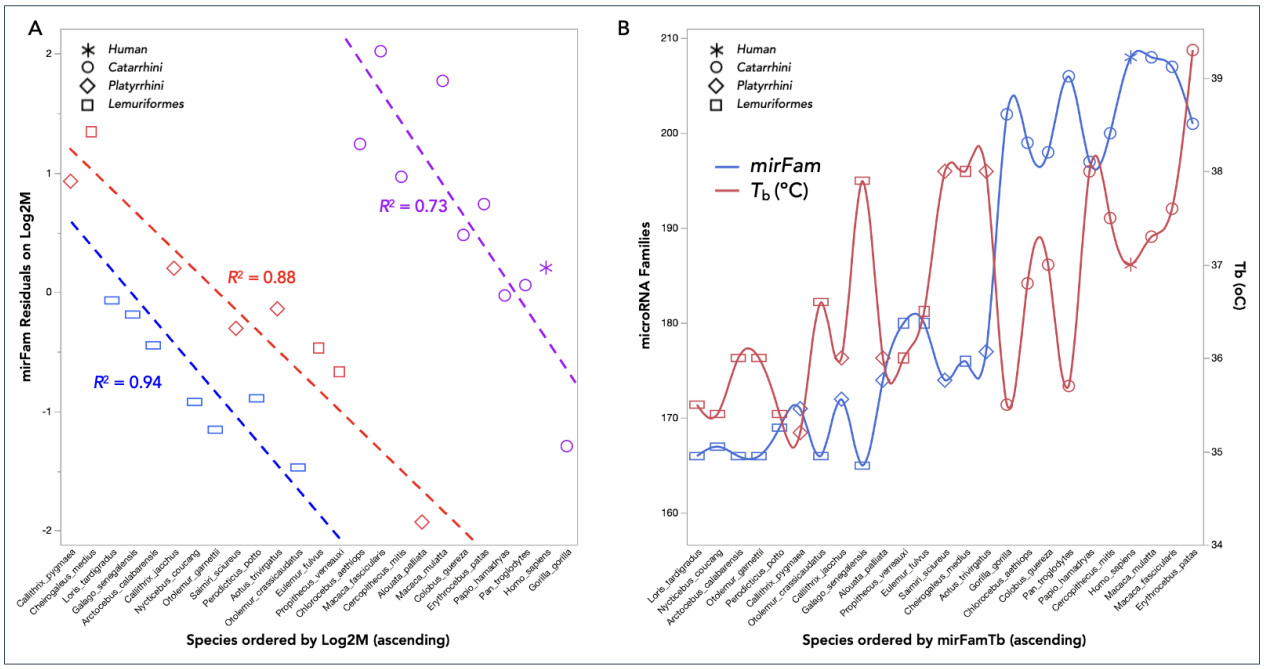

Figure S6. Conservation of *mirFam* and *mirFam* x T_b with respect to body size.
A. The *mirFam*-$\log_2 M$ relationship is least conserved among Catarrhini.
B. Visualization of the reciprocal variation of *mirFam* and T_b.

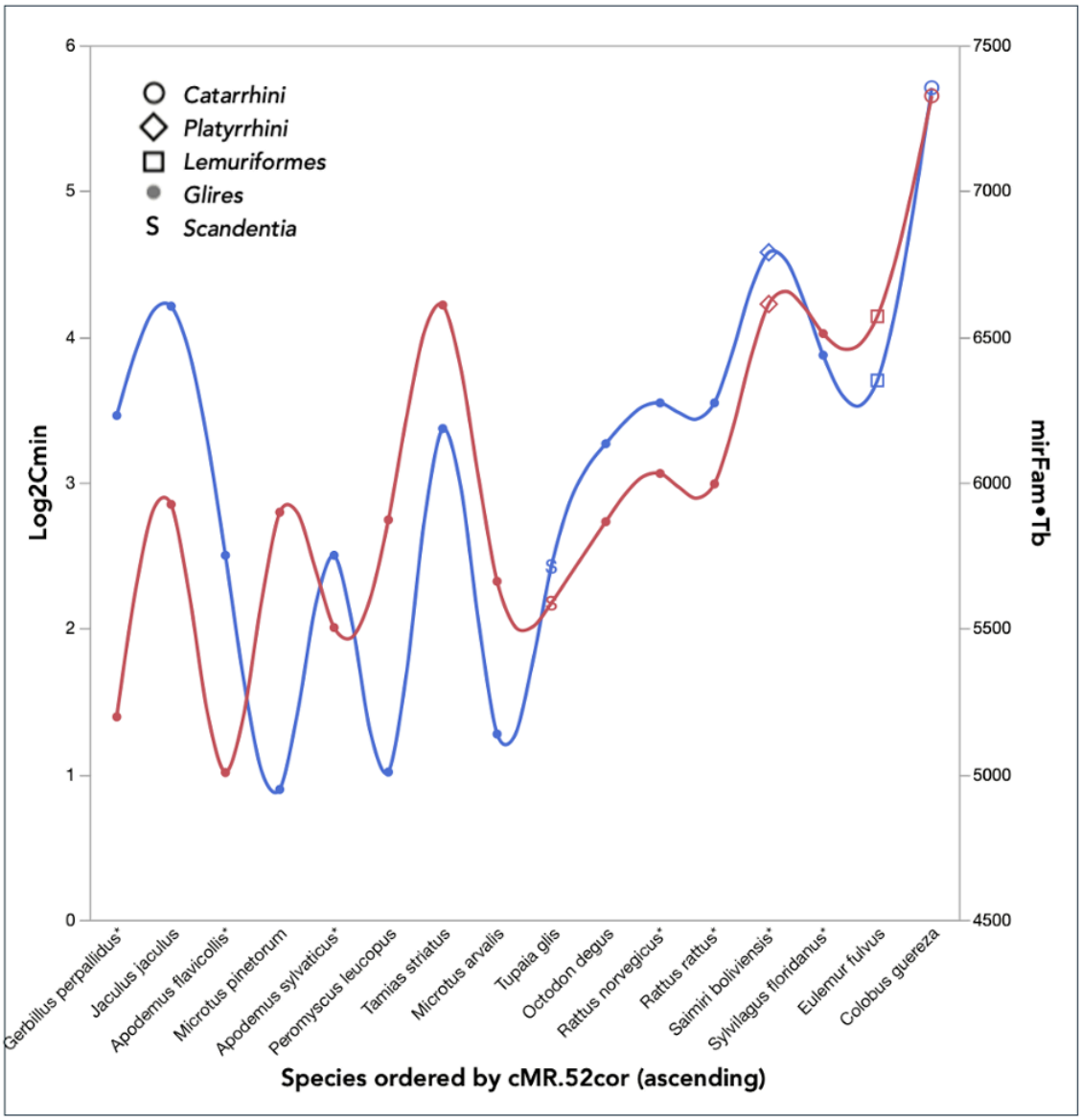

Figure S7. When ordered according to the rate of core thermogenesis (*cMR.52cor*), *mirFam•*T_b (red) generally tracks thermal conductance (blue). Asterisks (*) represent species in the 4-organ dataset of Wang et al (2012) that were substituted for congeneric species in the C_{min} dataset of Khaliq et al (2014) (see Methods for details).

	Allometric Exponent	Pagel's *lambda*	R^2	*P*	*AICc*
KIDNEY	0.80	0	0.5366	6.39E-05	-42.7
	0.75	0	0.5834	2.14E-05	-20.09
	0.70	0	0.5958	1.56E-05	-0.93
	0.65	0	0.5946	1.61E-05	16.22
	0.60	0	0.5859	2.00E-05	32.13
		Pagel's *lambda*	R^2	*P*	*AICc*
HEART	0.80	0	0.4937	1.60E-04	-38.02
	0.75	0	0.6476	3.83E-06	-17.88
	0.70	0	0.6962	8.44E-07	0.63
	0.65	0	0.7133	4.69E-07	17.65
	0.60	0	0.7163	4.21E-07	33.66
		Pagel's *lambda*	R^2	*P*	*AICc*
LIVER	0.80	0	0.5724	2.79E-05	-15.22
	0.75	0	0.4011	9.28E-04	-10.98
	0.70	0	0.0854	1.01E-01	-2.86
	0.65	0	-0.0344	5.89E-01	10.24
	0.60	0.962	0.0145	2.66E-01	27.34
		Pagel's *lambda*	R^2	*P*	*AICc*
BRAIN	0.80	1	0.0329	2.05E-01	-63.9
	0.75	1	0.107	7.55E-02	-35.75
	0.70	1	0.1336	5.07E-02	-10.58
	0.65	1	0.151	4.17E-02	11.76
	0.60	1	0.1596	3.71E-02	32.24

Supplementary Table S3. Summary of phylogenetic regressions of organ *cMR*s on *mirFam*.